INL/JOU-23-74827-Revision-0

Investigation of thermal hydraulic behavior of the High Temperature Test Facility's lower plenum via large eddy simulation

October 2023

Hyeongi Moon, SuJong Yoon, Mauricio Eduardo Tano Retamales, Aaron S Epiney, Minseop Song, Jae-Ho Jeong

Changing the World's Energy Future

INL/JOU-23-74827-Revision-0

Investigation of thermal hydraulic behavior of the High Temperature Test Facility's lower plenum via large eddy simulation

Hyeongi Moon, SuJong Yoon, Mauricio Eduardo Tano Retamales, Aaron S Epiney, Minseop Song, Jae-Ho Jeong

October 2023

Idaho National Laboratory
Idaho Falls, Idaho 83415

http://www.inl.gov

Prepared for the
U.S. Department of Energy
Under DOE Idaho Operations Office
Contract DE-AC07-05ID14517

Nuclear Engineering and Technology 55 (2023) 3874–3897

Contents lists available at ScienceDirect

Nuclear Engineering and Technology

journal homepage: www.elsevier.com/locate/net

Original Article

Investigation of thermal hydraulic behavior of the High Temperature Test Facility's lower plenum via large eddy simulation

Hyeongi Moon [a, b], Sujong Yoon [b], Mauricio Tano-Retamale [b], Aaron Epiney [b], Minseop Song [c, **, 1], Jae-Ho Jeong [a, *, 1]

[a] Department of Mechanical Engineering, Gachon University, 1342, Seongnam-daero, Sujeong-gu, Seongnam-si, Gyeonggi-do, South Korea
[b] Idaho National Laboratory, 2525 Fremont Ave., Idaho Falls, ID, 83415, United States
[c] Department of Nuclear Engineering, Hanyang University, 222, Wangsimni-ro, Seongdong-gu, Seoul, South Korea

ARTICLE INFO

Article history:
Received 30 April 2023
Received in revised form
24 May 2023
Accepted 3 July 2023
Available online 05 July 2023

Keywords:
CFD
VHTR
Jet mixing
Vortex core visualization
HTGR

ABSTRACT

A high-fidelity computational fluid dynamics (CFD) analysis was performed using the Large Eddy Simulation (LES) model for the lower plenum of the High–Temperature Test Facility (HTTF), a ¼ scale test facility of the modular high temperature gas-cooled reactor (MHTGR) managed by Oregon State University. In most next–generation nuclear reactors, thermal stress due to thermal striping is one of the risks to be curiously considered. This is also true for HTGRs, especially since the exhaust helium gas temperature is high. In order to evaluate these risks and performance, organizations in the United States led by the OECD NEA are conducting a thermal hydraulic code benchmark for HTGR, and the test facility used for this benchmark is HTTF. HTTF can perform experiments in both normal and accident situations and provide high-quality experimental data. However, it is difficult to provide sufficient data for benchmarking through experiments, and there is a problem with the reliability of CFD analysis results based on Reynolds–averaged Navier–Stokes to analyze thermal hydraulic behavior without verification. To solve this problem, high-fidelity 3-D CFD analysis was performed using the LES model for HTTF. It was also verified that the LES model can properly simulate this jet mixing phenomenon via a unit cell test that provides experimental information. As a result of CFD analysis, the lower the dependency of the sub-grid scale model, the closer to the actual analysis result. In the case of unit cell test CFD analysis and HTTF CFD analysis, the volume-averaged sub-grid scale model dependency was calculated to be 13.0% and 9.16%, respectively. As a result of HTTF analysis, quantitative data of the fluid inside the HTTF lower plenum was provided in this paper. As a result of qualitative analysis, the temperature was highest at the center of the lower plenum, while the temperature fluctuation was highest near the edge of the lower plenum wall. The power spectral density of temperature was analyzed via fast Fourier transform (FFT) for specific points on the center and side of the lower plenum. FFT results did not reveal specific frequency-dominant temperature fluctuations in the center part. It was confirmed that the temperature power spectral density (PSD) at the top increased from the center to the wake. The vortex was visualized using the well-known scalar Q-criterion, and as a result, the closer to the outlet duct, the greater the influence of the mainstream, so that the inflow jet vortex was dissipated and mixed at the top of the lower plenum. Additionally, FFT analysis was performed on the support structure near the corner of the lower plenum with large temperature fluctuations, and as a result, it was confirmed that the temperature fluctuation of the flow did not have a significant effect near the corner wall. In addition, the vortices generated from the lower plenum to the outlet duct were identified in this paper. It is considered that the quantitative and qualitative results presented in this paper will serve as reference data for the benchmark.

1. Introduction

The high-temperature gas-cooled reactor (HTGR) is one of six next generation nuclear plants (NGNPs) proposed by the Gen IV International Forum (GIF). HTGR has the advantage of being

* Corresponding author.
** Corresponding author.
E-mail addresses: hysms@hanyang.ac.kr (M. Song), jaeho.jeong@gachon.ac.kr (J.-H. Jeong).
[1] Minseop Song and Jae-Ho Jeong equally contributed to this work as corresponding authors.

https://doi.org/10.1016/j.net.2023.07.003
1738-5733/

Nomenclature

η	Kolmogorov scale
λ	Taylor's microscale
Δs	Cell size
k	Turbulence kinetic energy
ε	Turbulence dissipation rate
ν	Dynamic viscosity
sgs	Sub-grid scale
ρ	Density
Δ	Length scale or grid filter width
S_w	Deformation parameter for WALE sgs model
C_w	WALE model coefficient
κ	Von Karman constant
$\boldsymbol{v}$	velocity
$\mathbf{I}$	identity tensor
Q	Q-criterion
$\boldsymbol{\Omega}$	antisymmetric components of ∇u
$\boldsymbol{S}$	symmetric components of ∇u

suitable to thermally couple with high temperature industries or hydrogen production as the helium temperature of the cooling cycle reaches over 700 °C. In the case of the Very High Temperature Reactor (VHTR), which is the next step of HTGR, the target outlet temperature is set to 950 °C. The advantages of these high outlet temperatures in favor of mass production of hydrogen are being re-examined. Addressing several performance and safety issues related to thermal hydraulics in VHTRs identified in a comprehensive report published in 2002 is critical to the mission's success [1]. As mentioned in Phenomena Identification And Ranking Table (PIRT), excessive thermal gradients may lead to structural problems, and hot streaking can cause problems in downstream turbines or intermediate heat exchangers [2]. Sal et al. [3] investigated numerically the potential removal of hot streaks and stratification in the VHTR lower plenum using a helicoid insert. It was confirmed that the jet injected into the lower plenum through a bypass equipped with a helicoid insert reduced the phenomenon of collision with the bottom of the lower plenum and spread in a spiral shape. However, it is necessary to study the pressure drop and installation method of the helicoid insert. A study on the thermal mixing enhancement method of the lower plenum outlet duct to solve the mixing problem is also being conducted [4]. McEligot and McCreery [5] presented a conceptual design of an experiment for computational fluid dynamics (CFD) evaluation using the Matched-Index-of-Refraction (MIR) flow system developed by Idaho National Laboratory (INL), and Condie et al. [6] developed an experiment for CFD assessment using the MIR flow system. Richard [7] performed 2D Reynolds-averaged Navier-Stokes (RANS) and 2D unsteady Reynolds-averaged Navier-Stokes (URANS) CFD analyzes for a geometry similar to the lower plenum of a gas-cooled high temperature reactor. As a result of the analysis, a lesson was learned that adopting URANS predicts the average variable and total shear stress well. Guillen [8] performed a CFD analysis of an experiment using k-ε turbulence model. The experiment consists of eight inlet jet ports at the top of five cylindrical pillars and ten half pillars symmetrically arranged along two parallel sidewalls. However, these experiments are all experiments on simplified cases. In addition, due to the limitation of computational resources, the CFD analysis for a simple case was analyzed using a model with high turbulence model dependency. With the support of the U.S. Department of Energy (US-DOE), the High Temperature Test Facility (HTTF) [9] at Oregon State University is designed to experimentally investigate

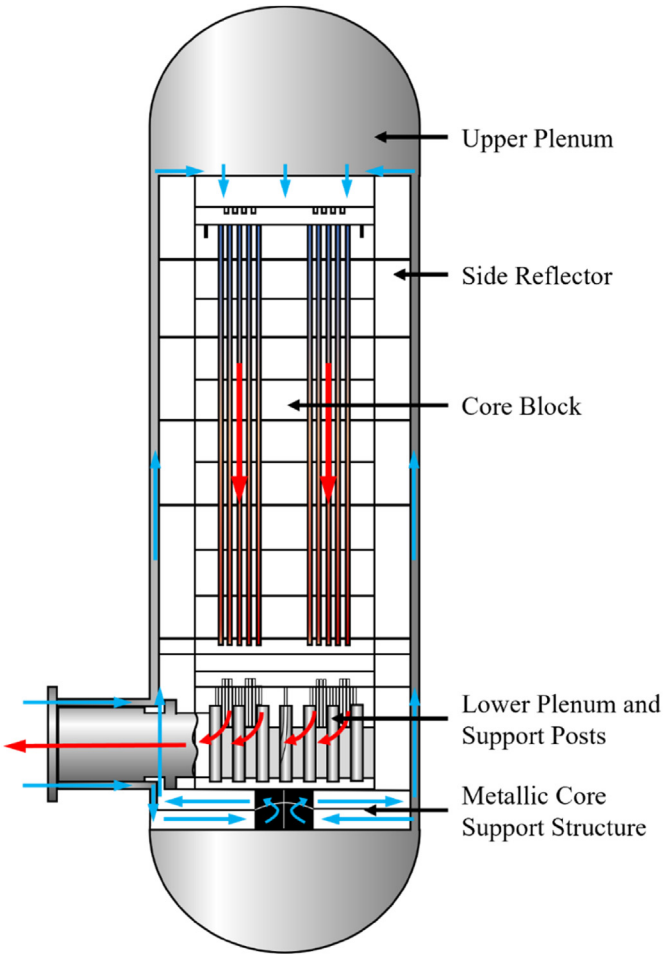

Fig. 1. Sectional view of overall HTTF cooling system using Helium gas.

Table 1
Helium properties used for CFD.

Dynamic viscosity [Pa·s]	1.9891
Molecular weight [kg/kmol]	4.0026
Specific heat [J/kg-K]	5197.61
Thermal conductivity [W/m-K]	0.154933
Turbulent Prandtl number	0.9

transient behavior in the high-temperature prismatic-type gas cooled reactors. This integral effect test (IET) facility is 1/4 scaled-down model of the General Atomic MHTGR [10]. This facility provides the experimental data for the code verification and validation (V&V) of the system thermal-hydraulics codes, CFD codes, and system-CFD code coupling. Individual modeling efforts for the HTTF data have been on-going at various international laboratories and universities. For instance, Gutowska and Woods [11] investigated the inlet plenum flow distribution during the normal operation condition. K. Podila et al. [12] investigated the entire system analysis by coupling RELAP5-3D, the system code, and STAR-CCM+ [13], a commercial CFD code. In order for the consistent analysis among different international modeling teams, the HTTF thermal hydraulics benchmark has been proposed to the OECD Nuclear Energy Agency (NEA). This benchmark aims to validate each participating organization's thermal-hydraulic codes using available high-fidelity HTTF laboratory measurements. The first exercise is to compare the results of the analysis using each code with a well-

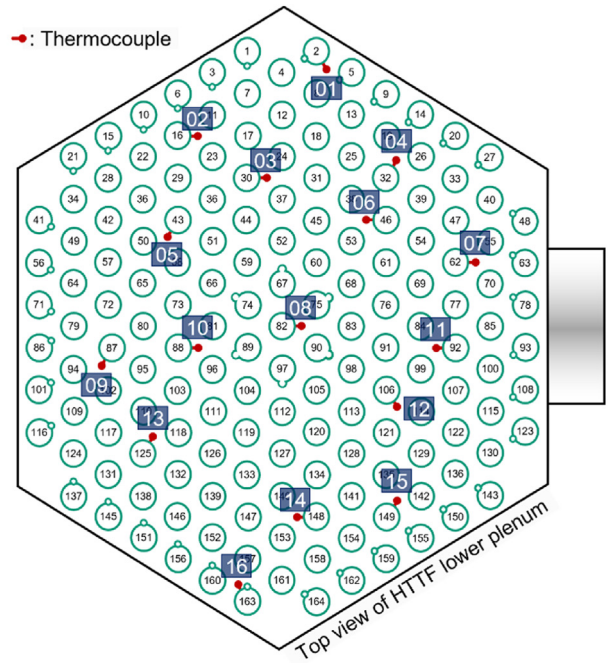

(A) Upper view of lower plenum and thermocouple locations

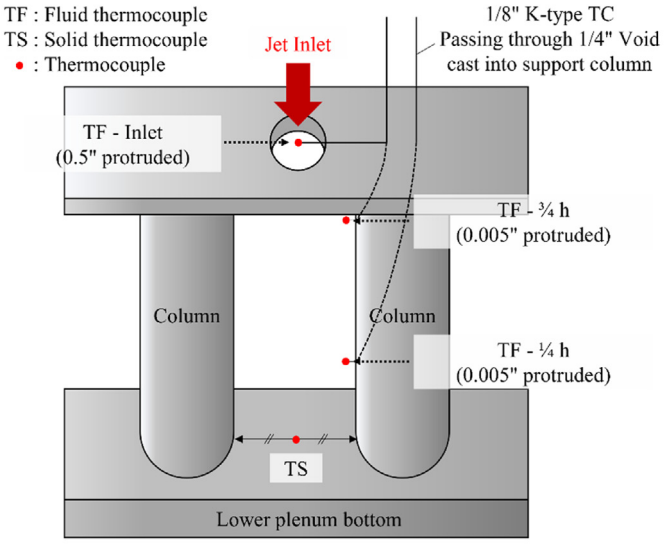

(B) Thermocouple mounting locations per jet characterization thermocouple module

Fig. 2. Lower plenum thermocouple location and number.

established fixed boundary condition to establish a base solution. To analyze the occurrence of the hot streaking problem, it is essential to study the thermal hydraulic behavior of helium gas inside the lower plenum. Although the HTGR is a mature reactor concept, the mixing phenomena occurring in the lower plenum remain poorly understood. However, it is difficult to predict the exact thermal hydraulic behavior inside the lower plenum only with the thermocouple and gas concentration instruments (GCI) data of the HTTF. Therefore, it is necessary to provide quantitative reference data for establishing a base solution through CFD analysis.

LES simulates large eddies and models SGS eddies to provide simulation results with lower model dependency. The URANS model can provide only data with a relatively large model dependency by modeling all eddies. The accuracy issue of the prediction of thermal fluctuations of URANS and LES for mixing of jets with different temperatures can be reviewed in Refs. [14,15]. Yu et al. performed CFD analysis using URANS and LES models for the triple jet experiment. Compared with the CFD analysis results, the URANS model also provided reasonable prediction results, but the LES model predicted the deviation of temperature and temperature fluctuation intensity more accurately than the URANS model [14]. S.

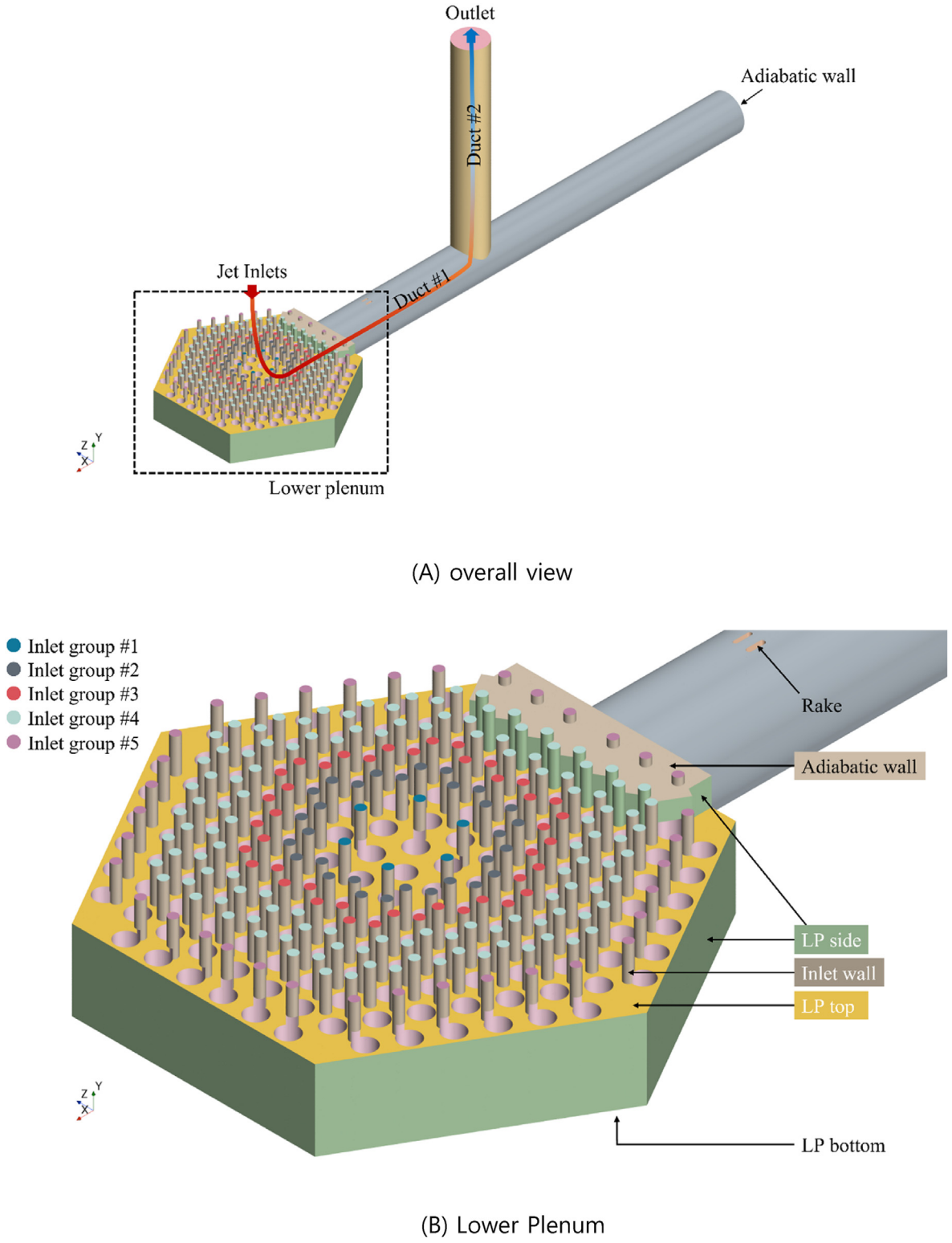

Fig. 3. HTTP lower plenum simulation domain view.

Chacko et al. compared the results of the triple jet experiment and the LES calculation, and found that the LES model predicts jet mixing well and the temperature fluctuations agree well with the experimental results, which is essential information to analyze the thermal striping phenomenon [15]. D. Tyler Landfried [16] analyzed the phenomenon occurring in the lower plenum through the unit cell test of the VHTR lower plenum. Corey E [17] performed CFD analysis using URANS for the lower plenum, and Sasan S [18]

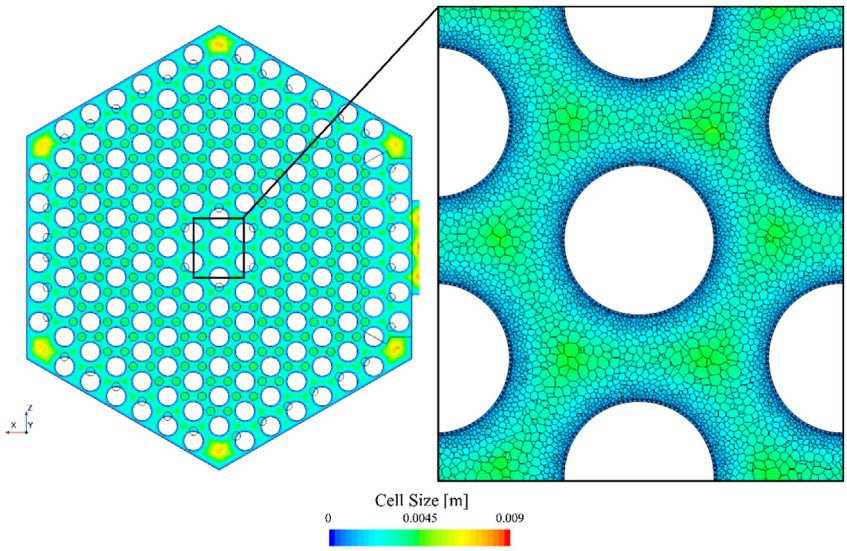

Fig. 4. Cell size contour in the 50% height sectional plane of the LP.

Table 2
Computing grid specifications for HTTF LES analysis.

Cell type	Polyhedron, Prism layer
Base size [mm]	0.9
Number of prism layer	1
Thickness of prism layer [mm]	0.9
Number of cells	70 million
Maximum cell size [mm]	25.4
Volume averaged cell size [mm]	6.28

Table 4
CFD solver settings for unit cell test.

Simulation tool	Star-CCM+
Simulation type	3D, Implicit-unsteady
Turbulence model	LES
SGS model	WALE
Convection scheme	Bounded-central
Convective Courant number	≤ 1
Temporal discretization	Second-order
Total simulation time	$>10 \times T_{FT}$
Inner loop iteration	10

qualitatively compared the unit cell test results of VHTR with the LES results. Kimber et al. [19] quantitatively compared the LES analysis result and the experimental result for the unit cell test, but this has the limitation of the unit cell test, and thermal hydraulic analysis of the entire lower plenum was not performed. The main goal of this study is to accurately simulate the thermal hydraulic behavior for the entire HTTF lower plenum through high-fidelity CFD using the LES model and to provide data that can be a reference for code-code comparison analysis. To verify the CFD calculation methodology, the CFD calculation for the Unit Cell Test was performed and compared with the experimental results. By applying the verified CFD calculation methodology, the LES model applied CFD calculation for HTTF was performed. The vortex core was visualized through vortex identification to understand the overall behavior of the helium gas in the lower plenum. The mixing of hot and cool helium gas was analyzed with the temperature fluctuation characteristics mainly for the thermocouple attached columns in the lower plenum. In addition, analysis in the frequency domain was performed using Fast Fourier Transform (FFT). The potential occurrence of thermal striping near the support structures and edges of lower plenums with large temperature fluctuations was also analyzed.

Table 3
Boundary conditions for HTTF LES analysis.

Wall	**Name**	**Condition**	**Temperature [K]**
	Duct Wall #1	No-slip	416.17
	Duct Wall #2		309.32
	Lower plenum side		435.71
	Lower Plenum Bottom		476.88
	Lower Plenum Top		565.68
	Column Walls		518.26
	Extruded Inlet Wall		Adiabatic
	Rake		Adiabatic
Inlet	**Name**	**Mass flow rate [kg/s]**	**Total Temperature [K]**
	Inlet #1	1.30E-3	562.22
	Inlet #2	9.83E-3	561.84
	Inlet #3	1.48E-2	541.34
	Inlet #4	1.54E-2	512.03
	Inlet #5	4.67E-3	471.64
Outlet	**Name**	**Gauge pressure [Pa]**	**Static temperature [K]**
	Outlet	110486.05	501.25

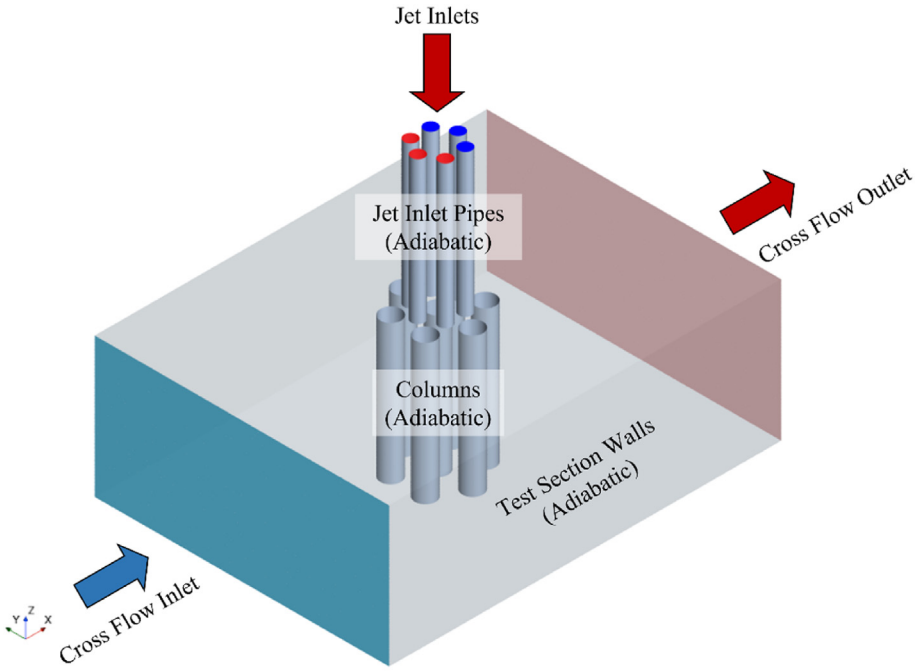

(A) Full domain

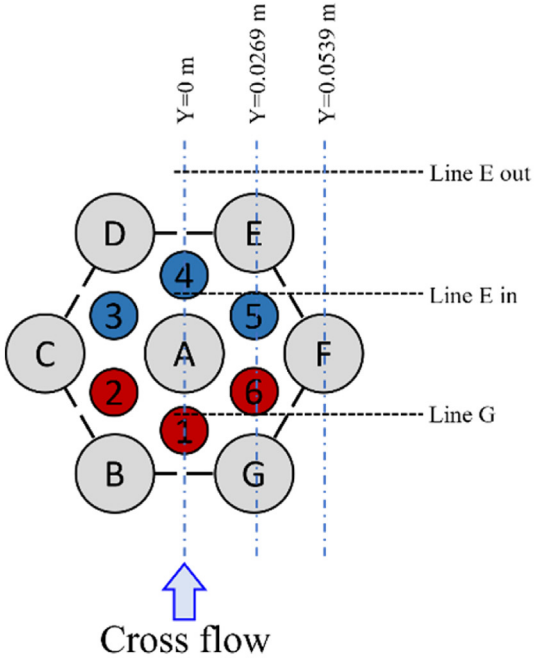

(B) Data acquisition line

Fig. 5. Simulation domain and data measurement location for unit cell test.

2. Computational study of flow in HTTF lower plenum on normal operation

Prior to CFD analysis, it is essential to select a suitable turbulence model for the analysis target. In the case of laminar-dominant flow, the turbulence model application is not appropriate due to the fact that there's no viscosity caused by turbulent flow. For turbulent dominant flow, application of turbulence models such as URANS and LES is considered, and if computational resources are sufficient, direct numerical simulation (DNS) can also be performed. RANS has

Table 5
Boundary conditions of the unit cell test Case I.

Case	Boundary	Mean Inlet Temperature, $\overline{T}_{inlet}$ [°C]	Mass flow rate, $\dot{m}$ [kg/s]
Case I	Cross flow	298.39	1.471792
	Jet 1	356.41	0.002955
	Jet 2	348.16	0.003069
	Jet 3	314.34	0.001774
	Jet 4	312.48	0.002956
	Jet 5	307.77	0.003102
	Jet 6	343.11	0.001851
	Outlet	**Gauge pressure [pa]**	**Target mass flow rate, $\dot{m}$ [kg/s]**
	Outlet	0	1.487499
	Wall	**Thermal condition**	**Friction condition**
	All walls	Adiabatic	No-slip

Table 6
CFD solver settings for Unit Cell Test and HTTF lower plenum.

Simulation tool	Star-CCM+
Simulation type	3D, Implicit-unsteady
Turbulence model	LES
SGS model	WALE
Convection scheme	Bounded-central
Time step size [s]	1.0E-4
Temporal discretization	Second-order
Total simulation time	>2TFT
Inner loop iteration	10

Table 7
Cell count of Unit cell test according to Δs.

Base Size (Δs) [mm]	Number of Cells [million]
2.0	1.4
1.0	6.3
0.75	12.3
0.625	19.7
0.5	33.6

been widely used in existing studies because of its low resource cost, and many detailed models have been developed and verified [20–22]. However, the prediction accuracy of RANS model depends on the turbulent closure models. Furthermore, there is no universal mesh structure that is optimal for all turbulence models. Consequently, it is not desirable to fully trust the RANS model in the pure prediction stage where experimental results do not exist. Recently, due to the development of computing equipment, as LES and DNS level simulation that requires higher resources has become possible, many studies using the LES and DNS levels are being conducted. LES has low dependence on the turbulence model, so high-fidelity simulation is possible even without experimental results, and the required resources are reasonable compared to DNS. In this paper, the LES calculation for the unit cell test was performed for the evaluation of the LES calculation methodology, and the LES analysis of the HTTF lower plenum was performed using the calculation methodology.

2.1. Numerical physics

In HTTF, jets with different temperatures and velocities pass through the prismatic core and flow into the lower plenum, resulting in a complex mixing phenomenon due to the complicated flow path. To calculate these turbulent behaviors, transient analysis is required and turbulent models such as URANS, LES, or DNS must be selected. The range of cell sizes commonly used for the DNS model to resolve Kolmogorov scale turbulence is as below where η indicates Kolmogorov scale, and Δs represents cell size (m).

$$\frac{1}{2}\eta \geq \Delta s$$

Where ν, k and ε indicates dynamic viscosity, turbulence kinetic energy and turbulence dissipation rate, respectively, the definition of η_ε in the ε model is:

$$\eta_\varepsilon = \sqrt{10\nu\frac{k}{\varepsilon}}$$

The cell size for LES analysis is desirable to form an inertial subrange in which an energy cascade occurs and the energy decreases at a rate of −5/3. In this way, the range of cell sizes suitable for the LES model can be represented as below through Taylor's microscale, λ.

$$\lambda \geq \Delta s \geq \eta$$

In the ε model is, the definition of λ_ε is:

$$\lambda_\varepsilon = \left(\frac{\nu}{\varepsilon}\right)^{\frac{1}{2}}$$

In a simple case, λ and η can be calculated by calculating the turbulence length scale and turbulent intensity through the well-known estimating equation, but it is difficult to use this method because the geometry of the HTTF lower plenum is complicated. Alternatively, λ and η can be calculated through RANS analysis. As a result of RANS calculation, volume averaged λ is calculated as 1.27E-2 m, and volume averaged η is calculated as 3.58E-3 m. As a result of this rough calculation, the number of cells required to perform DNS is 44.6 times that of LES. However, the method of setting the cell size based on these values does not satisfy the cell size required for the local region, which increases model dependency and may cause simulation results with low accuracy. To overcome the issue of setting Δs, M value can be adopted as a consequential cell size evaluation method. M value is defined as the ratio of modeled k and total k as shown in the following equation and can be evaluated after LES calculation.

$$M = \frac{k_{sgs}}{k_{resolved} + k_{sgs}}$$

The recommended M is less than 0.20, and if resources are sufficient, the calculation can be performed more accurately in the M value of less than 0.05 [13].

The sub-grid-scale model of LES was selected as the WALE model, which uses a novel form of velocity gradient tensor [23]. Like the Smagorinsky sub-grid-scale model, WALE model has the limitation that the model coefficients C_w are not universal [24]. However, validation using STAR-CCM + showed that the WALE model was less sensitive to the C_w value than the Smagorinsky

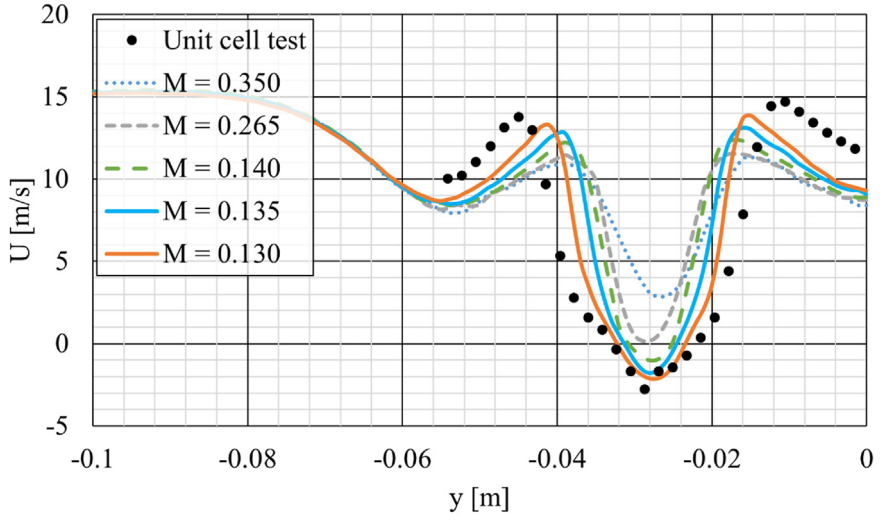

(A) Cross flow direction component

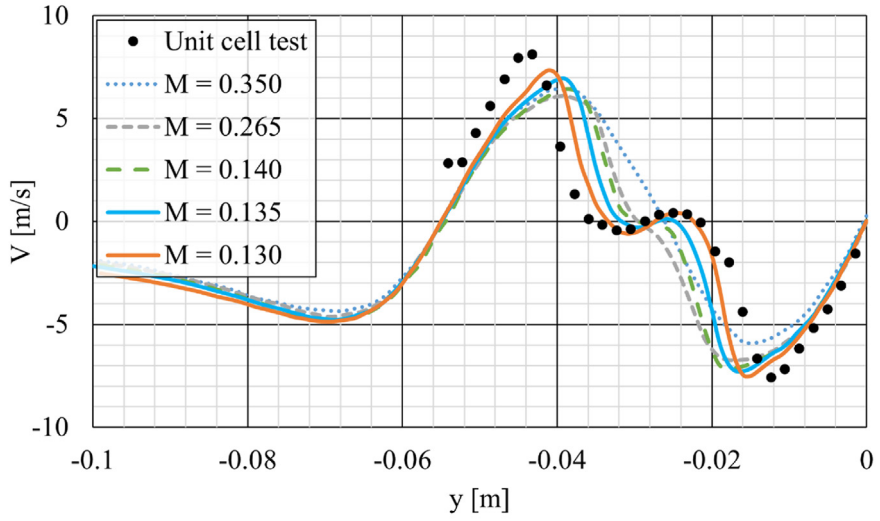

(B) Height component

Fig. 6. Measured and CFD calculated velocity at line G at 50% height.

model [13]. Another advantage of the WALE model is that it does not require any near-wall damping and provides accurate scaling at walls automatically. The WALE model provides the following formula for the sub-grid scale viscosity:

$$\mu_t = \rho \Delta^2 S_w$$

The deformation parameter is defined as:

$$S_w = \frac{S_d : S_d^{3/2}}{S_d : S_d^{5/4} + S : S^{5/2}}$$

$$S_d = \frac{1}{2}\left[\nabla v \bullet \nabla v + (\nabla v \bullet \nabla v)^T\right] - \frac{1}{3} tr(\nabla v \bullet \nabla v)\mathrm{I}$$

The model coefficient C_w is not universal and typical values of C_w reported in the literature range from 0.5 for homogeneous isotropic decaying turbulence to 0.325 for channel flow. Validations with STAR-CCM + have shown that the default value of 0.544 for C_w works well for both homogeneous isotropic decaying turbulence and channel flows (Star-CCM + User Guide). The simulation of this study was conducted by default, setting C_w to 0.544 and κ to 0.41.

2.2. Settings for CFD analysis of HTTF lower plenum

HTTF uses helium as a cooling gas. Flows into the upper plenum through the gap between the RPV wall and the reflector as shown in Fig. 1. The helium gas properties were set as constant, so that the benchmark participating organizations did not have to consider the difference in the interpolation method of the property values between codes. The constant properties of helium used for CFD are shown in Table 1. Helium gas from the upper plenum flows down from the top through the prismatic core. The helium gas injected into the lower plenum has a temperature difference at each inlet, so there is a concern that a hot striking phenomenon may occur during jet mixing. In order to analyze the thermal hydraulic

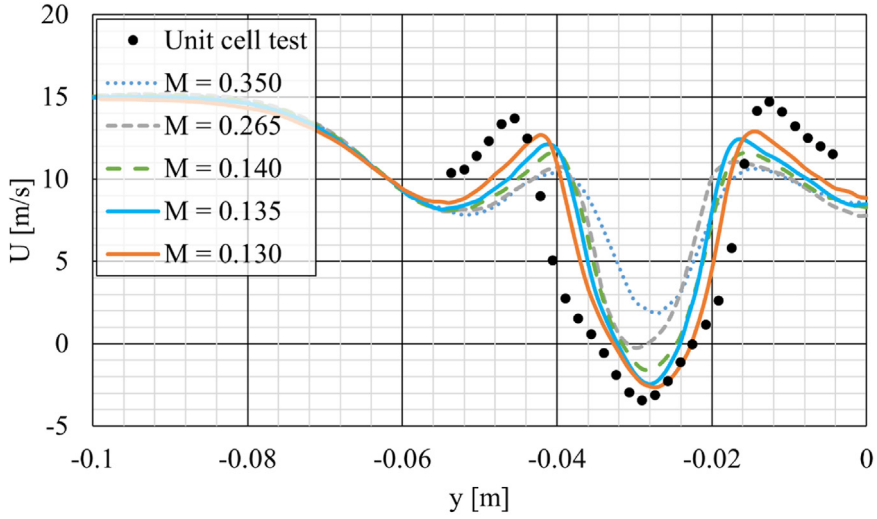

(A) Cross flow direction component

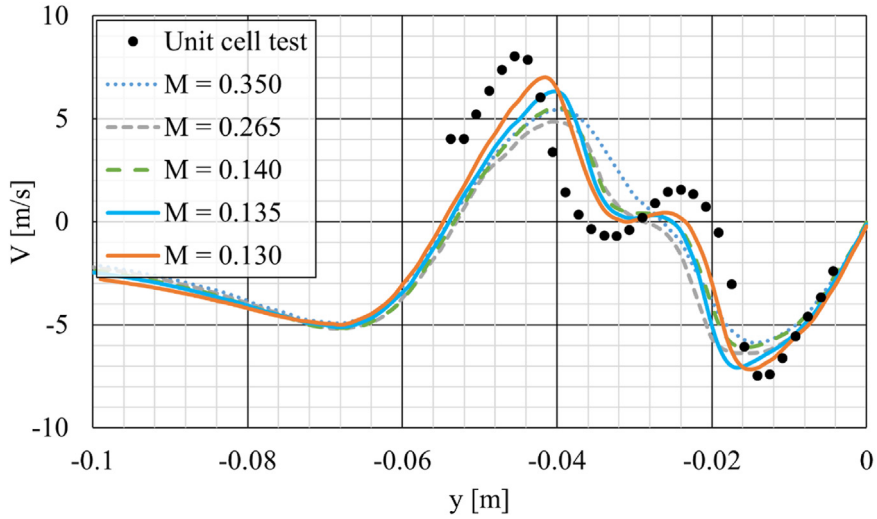

(B) Height component

Fig. 7. Measured and CFD calculated velocity along line G at 75% height.

phenomenon inside the lower plenum through experiments, thermocouples are installed on the supporting columns of the HTTF lower plenum as shown in Fig. 2(A) and (B). There are two types of thermocouple attachment methods. The first type has two fluid thermocouples installed in the column. The second type, the jet characterization thermocouple module, has an additional thermocouple installed to measure the jet inlet temperature and the solid temperature of the bottom, for a total of four thermocouple sets. A total of 4 first-type and 12 s-type thermocouple sets are installed in the HTTF lower plenum. The thermocouples installed on the columns to measure the fluid temperature protrude 0.127 mm from the wall, and the thermocouples to measure the jet inlet temperature are located at the center of the inlet.

2.2.1. Numerical analysis domain of HTTF lower plenum

Fig. 3 (a) and (b) show the overall view of the computational simulation domain of HTTF and the local view of the lower plenum, respectively. The scope of the simulation to be performed in this study is the region where the injected helium from the lower plenum passes through the outlet duct to the T-junction. The inlet group is divided into five, each with a different temperature and mass flow rate. Any helium jets that are injected into the lower plenum through the inlet group exit through the outlet duct. In the outlet plenum, the rake of the experimental device was implemented as it is to eliminate the difference in geometry from the actual test facility.

Fig. 4 shows the cell size and mesh formation for the section plane at the 50% height of the lower plenum. Large Eddy simulation was performed by configuring the size of the maximum cell corresponding to the lower plenum to be less than 5 mm, that is, less than about 6 times Δs, and the mixing phenomenon of jets ingress into the lower plenum was investigated. The mesh details are shown in Table 2. The maximum cell size among the entire grid is 25.4 mm. The volume average cell size is 6.28 mm. The boundary layer was formed with one prism layer, and the height was set to be the same as Δs, and all other polyhedral cells were used to form a grid.

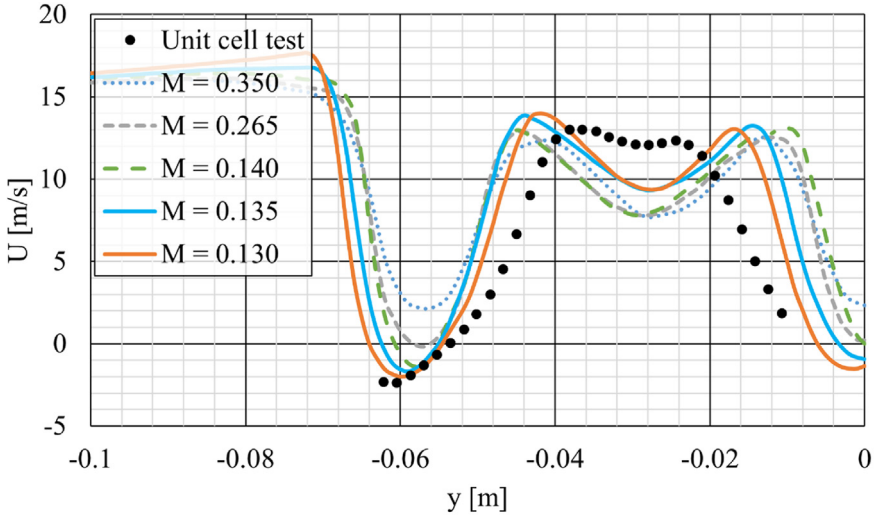

(A) Cross flow direction component

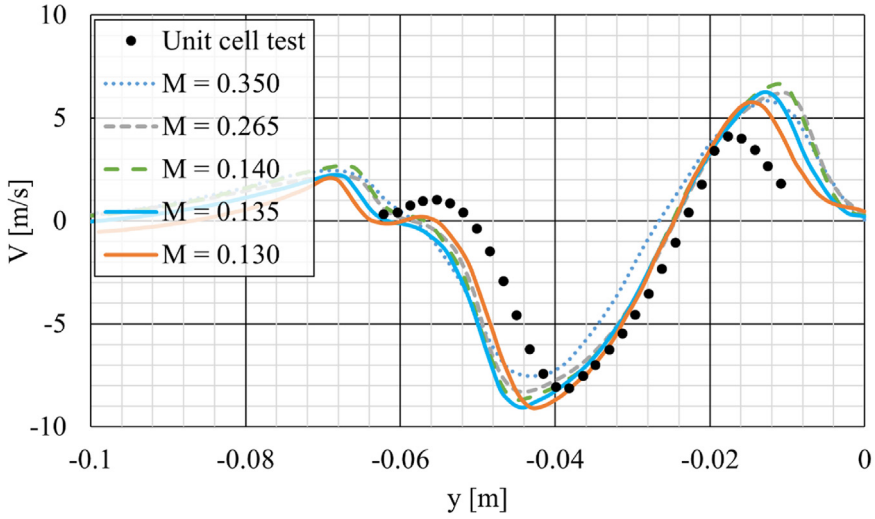

(B) Height component

Fig. 8. Measured and CFD calculated velocity at line E in at 50% height.

2.2.2. Boundary conditions of HTTF lower plenum

The purpose of this study is to find a base solution through apples-to-apples comparison of each participating organization. While many instruments are installed inside the HTTF and provide high-precision data, information such as the flow rate of helium has a large uncertainty in measurement. In this exercise, rather than performing analysis with precise boundary conditions, rough boundary conditions calculated through the RELAP5-3D system code based on the experimental results are used. The inlet boundaries are divided into five groups. The detailed boundary conditions are tabulated in Table 3. Among the adjacent inlets, #4 and #5 have the largest temperature difference of 40.383K. The outlet condition was set as a pressure outlet, and the target mass flow rate was set equal to the total inlet mass flow rate. The inlet wall, rake, and adiabatic wall were set to adiabatic conditions, and constant temperature conditions were set for the rest of the walls, and simulations were performed under no-slip conditions for all walls.

2.2.3. Solver settings for HTTF lower plenum

The solver settings are shown in Table 4. Large Eddy Simulation was performed using commercial software STAR-CCM+, sub-grid scale eddies were modeled with the WALE SGS model, and the convection scheme was adopted as a bounded-central method. The time step size was set to 1.0E-04 s, and the convective Courant number was calculated to be less than 1 in almost all cells. The total calculation time is 2 flow through time, which is the time of dividing the geometry volume by the volume flow rate. The inner loop is set to 10 times.

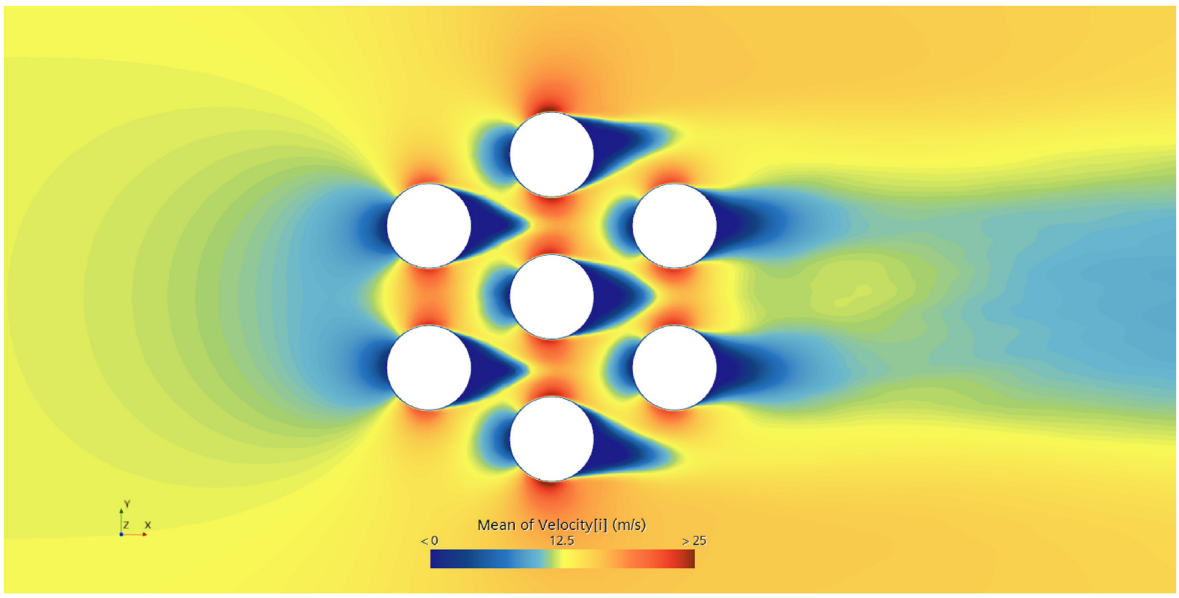

(A) Δs = 0.625 mm, M < 0.135

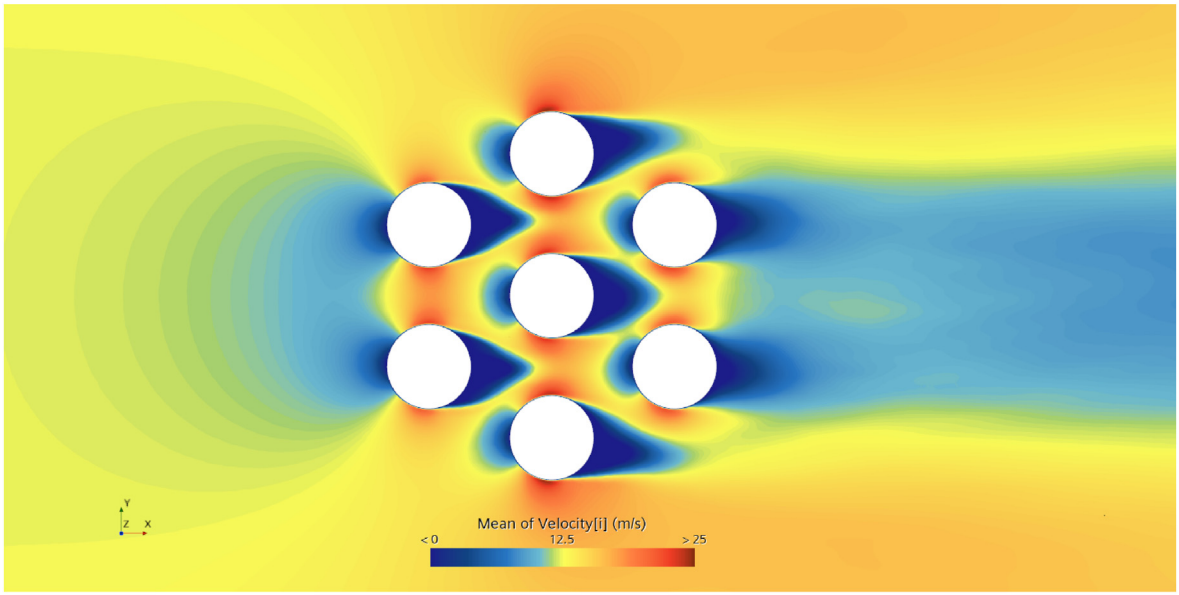

(B) Δs = 0.5 mm, M < 0.130

Fig. 9. Simulated mean x-velocity contour of 50% height section plane.

2.3. Settings for CFD analysis of unit cell test

D. Tyler Landfried et al. performed unit cell tests and investigated the mixing of jets flowing into the lower plenum of the VHTR. CFD analysis of HTTF is a large-scale simulation and requires a lot of computational resources and time. It is necessary to pre-examine the methodology by applying it to the unit cell test for VHTR lower plenum before large-scale calculation. In this process, the ratio modeled by the SGS model among the total turbulent kinetic energy have been used as an indicator. The accuracy of the CFD analysis for HTTF was evaluated by comparing the consistency with the experimental results according to the M.

2.3.1. Numerical analysis domain and boundary conditions of unit cell test

The unit cell test was performed through the wind tunnel, and the area of CFD analysis in this study included only the test section. The test section was designed with width, height, and length of 457.84, 217.42, and 609.60 mm, respectively. A total of 7 posts with a diameter of 31.75 mm and a total of 6 jet pipes with a diameter of 22.23 mm were installed. The jet length protrudes outside the test section by 615.95 mm. The test section area of the unit cell test is

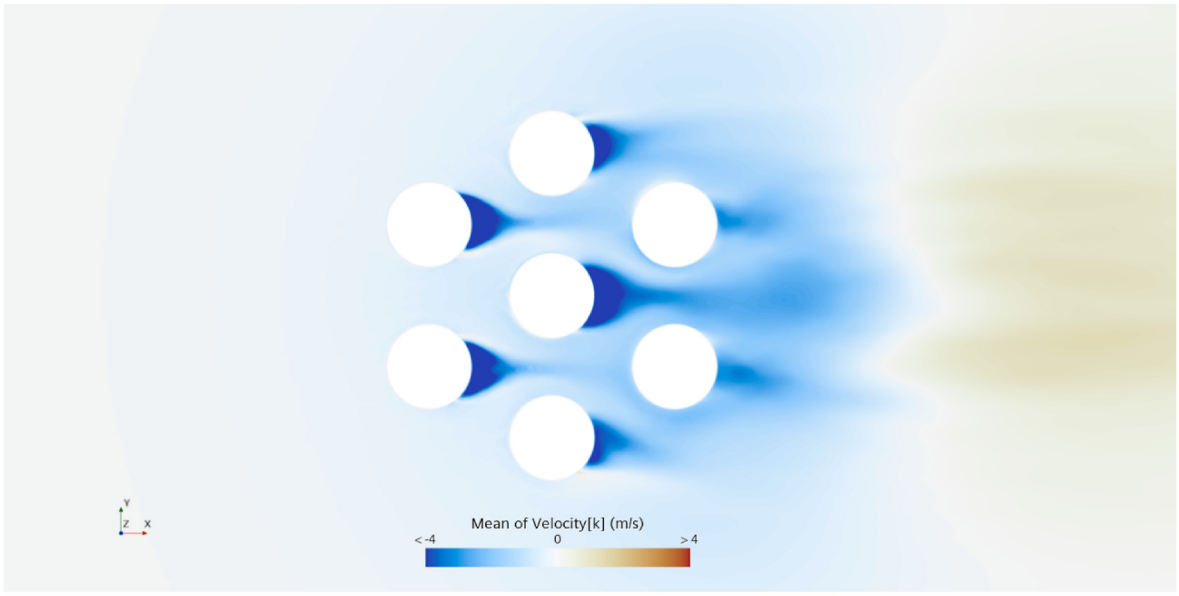

(A) Δs = 0.625 mm, M < 0.135

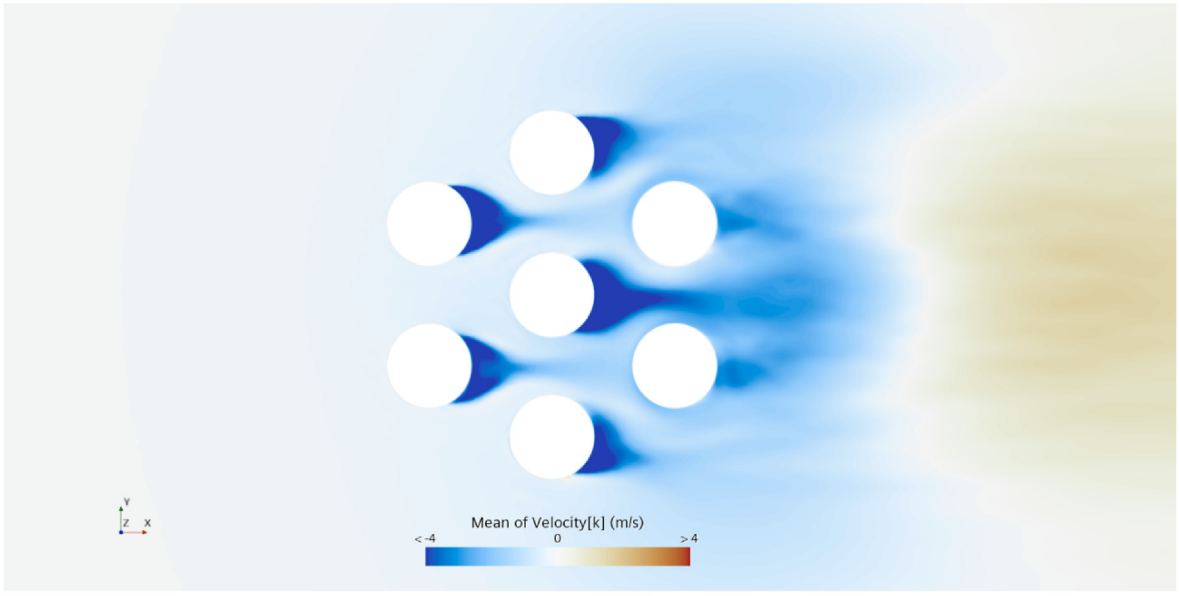

(B) Δs = 0.5 mm, M < 0.130

Fig. 10. Simulated mean z-velocity contour of 50% height section plane.

shown in Fig. 5. Six developed jets flow down from the top of the test section and cross flow along the wind tunnel across the test section.

The density was considered by setting the gas as an ideal gas, and all boundary conditions are shown in Table 5. The outlet was set as a pressure outlet, and all walls, including columns, were set to insulated and non-slip conditions.

One prism layer was formed on the wall with the simulation grid and the rest were formed with polyhedral cells, using the same algorithm as the grid used for HTTF lower plenum simulation.

2.3.2. Solver settings for unit cell test

The CFD solver settings are described in Table 6, and the same algorithm was used to test the settings to be applied to the HTTF simulation. The LES model was performed by setting Δs to 2 mm, 1 mm, 0.75 mm, 0.625 mm, and 0.5 mm, and a sensitivity study was conducted by comparing the simulation results with the experimental results according to the difference in M value. The time step size was set differently in proportion to the cell size in order not to change the convective Courant number.

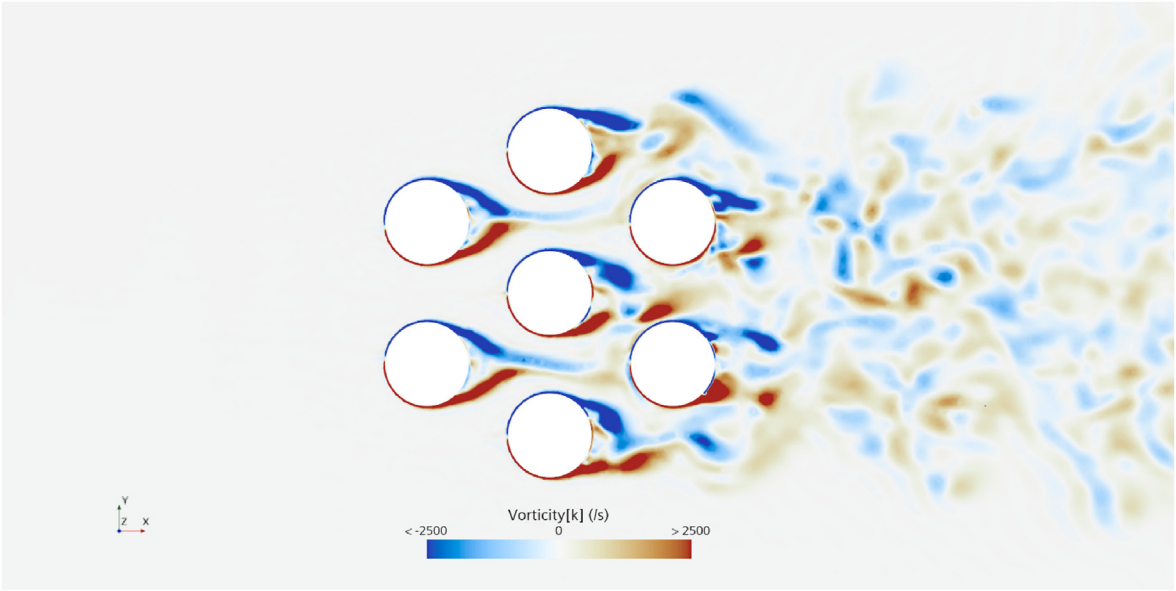

(A) Δs = 0.625 mm, M < 0.135

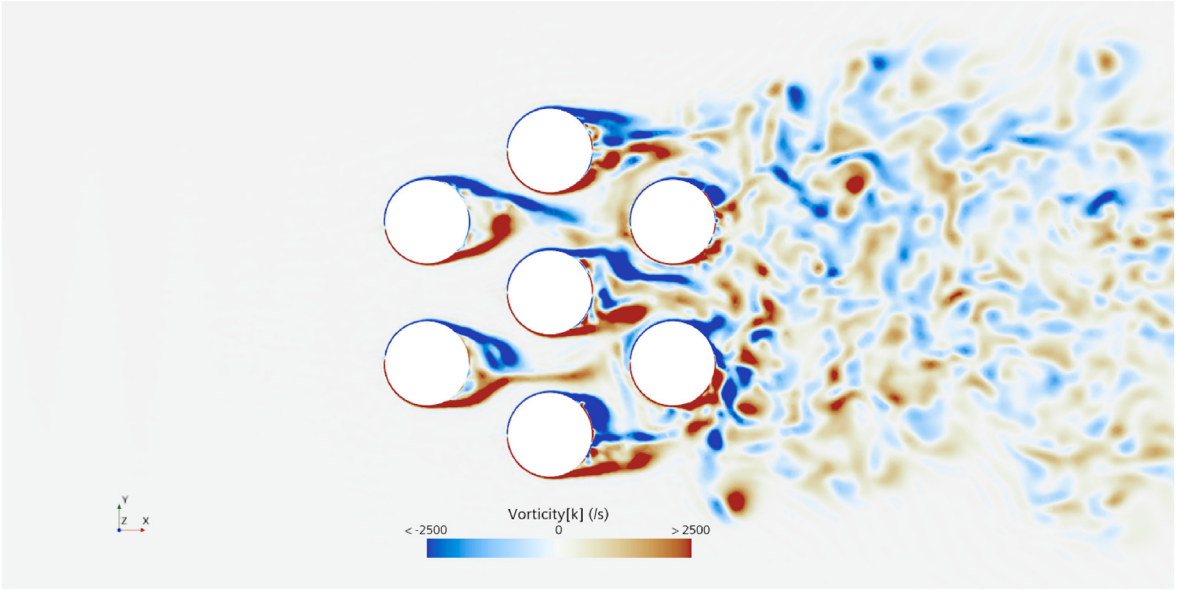

(B) Δs = 0.5 mm, M < 0.130

Fig. 11. Simulated z-vorticity contour of 50% height section plane at 10 T_{FT}.

3. CFD results analysis of unit cell test

A CFD analysis was performed on the unit cell test, and the velocity profile according to the measurement height in each measurement line was compared with the velocity profile calculated through CFD.

3.1. CFD results analysis and comparison with experimental data

LES analysis was performed on the unit cell test, and the time step size was set by calculating the convective Courant number to be less than 1. Poly cells for simulation were formed by changing Δs, and the resulting number of grids is shown in Table 7.

The calculation was carried out during the total simulation time of 5 flow through time. The calculated velocity profile and the velocity profile measured through experiments were compared in Figs. 6–8. Both cross-flow direction and height-direction velocity profiles agree well with the experimentally measured velocity profiles with increasing M values. It was also confirmed to directly predict the negative velocity profile due to wakes occurring after post G at both 50% and 75% heights.

Compared with the crossflow direction velocity component at line E at 50% height, there was some error from the experiment results. However, reducing the M value improved the prediction of the peak position and the y-velocity. As a result, it was confirmed that the lower the M, the better the agreement with the

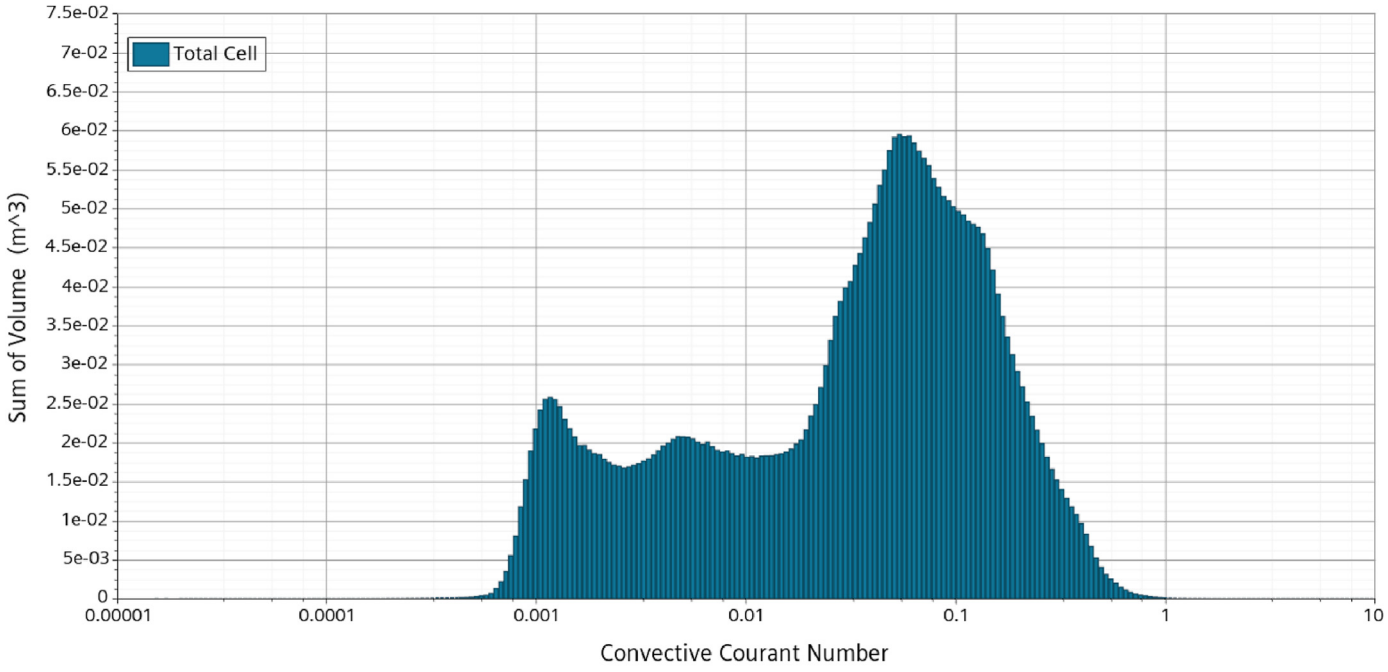

(A) Convective Courant number

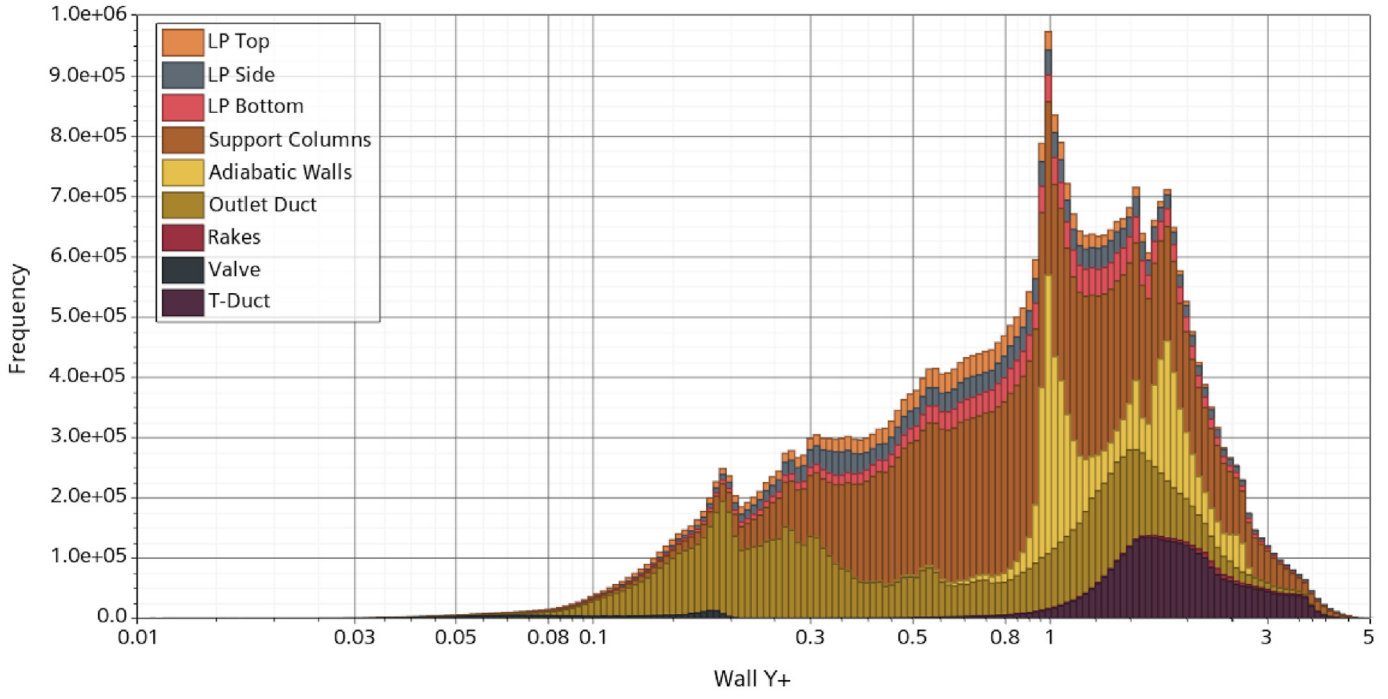

(B) Wall Y+

Fig. 12. Calculated Courant number and y plus of HTTF lower plenum large eddy simulation.

experimental results. The calculated volume averaged M value in this simulation is less than 13%.

Figs. 9–11 shows the mean velocities in the x- and z-directions and temporal z-vorticity measured for 10 flow through time. It was confirmed through the mean x-velocity contour that the flow separation area behind the column increased as Δs decreased. When Δs is the smallest case, 0.5 mm, the flow separation area is calculated to be larger than when it is 0.625 mm. Through the z-direction velocity contour in Fig. 10, it was found that the cell size should be sufficiently small to prevent underestimation of the effect of the jet. The z-direction vorticity contour in Fig. 11 shows that small eddies that flow between columns can be simulated only

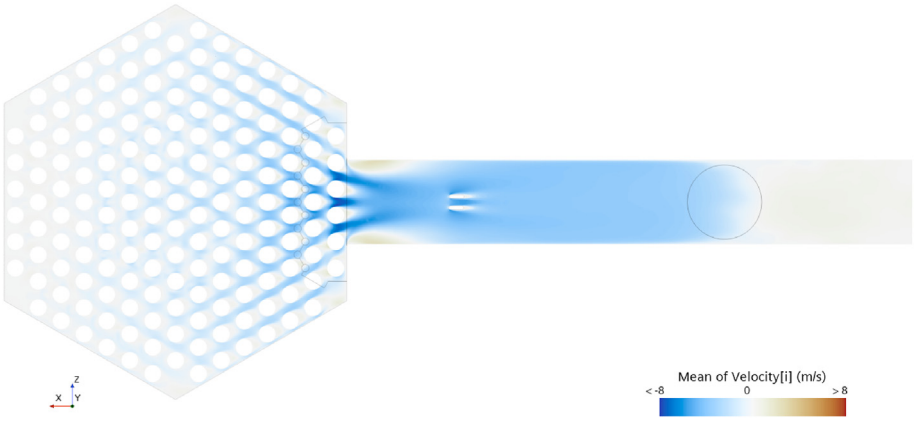

(A) x-Velocity

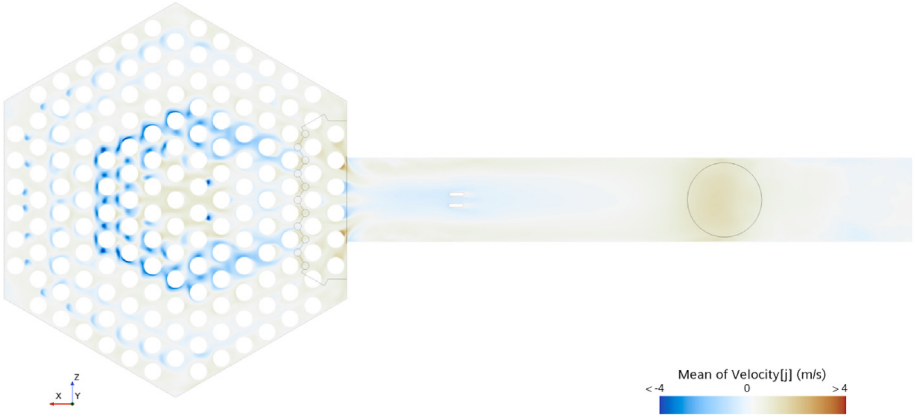

(B) y-Velocity

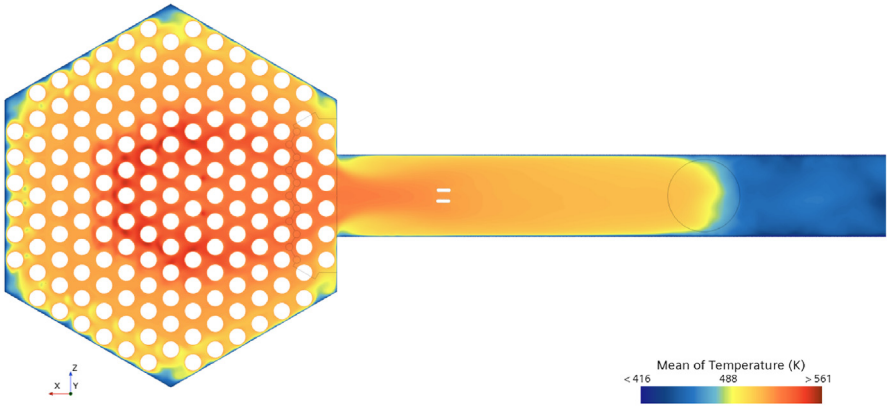

(C) Temperature

Fig. 13. Temperature variance contour at 25, 50, 75% height of lower plenum.

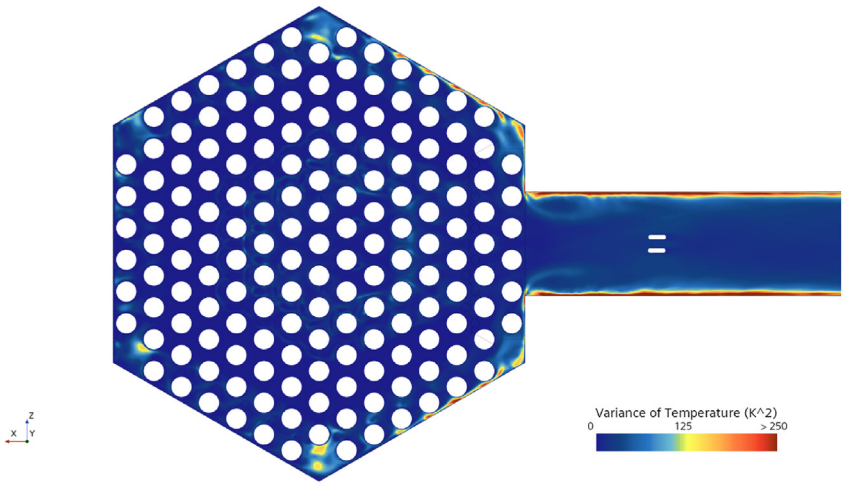

(A) 75% height

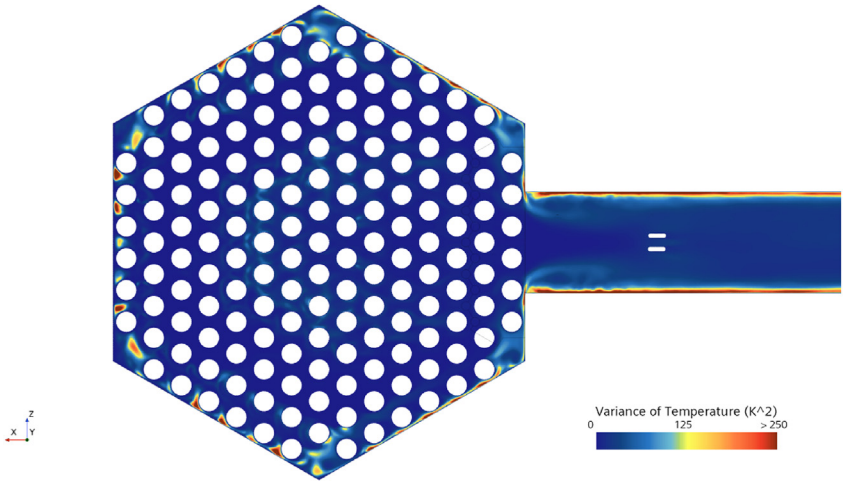

(B) 50% height

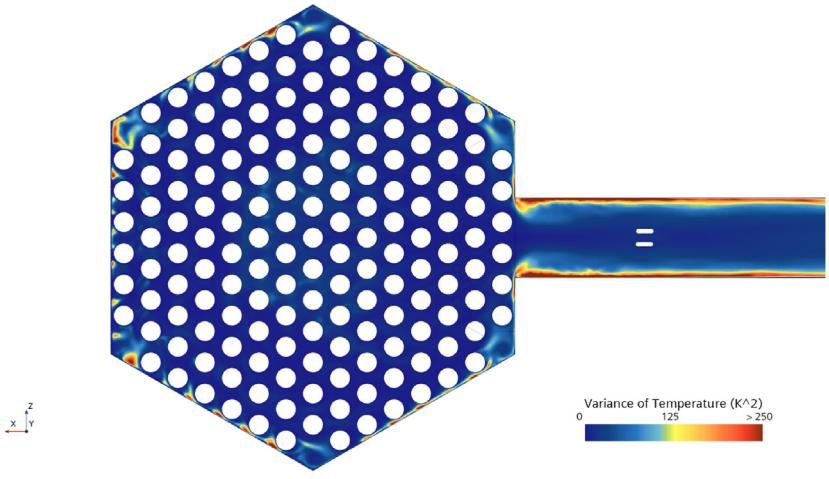

(C) 25% height

Fig. 14. Temperature variance contour at 75, 50, 25% height of lower plenum.

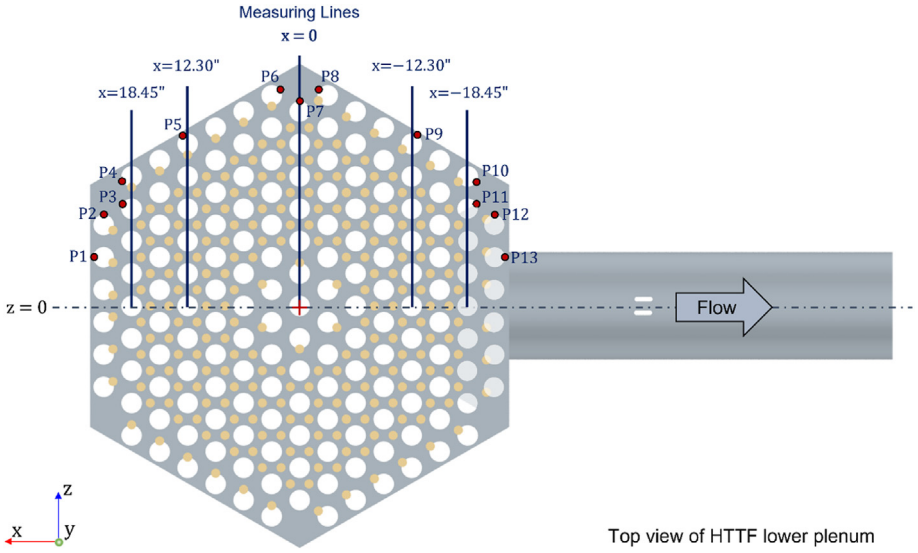

Fig. 15. Measurement lines and points of the HTTF lower plenum.

when the cell size is set small enough to increase the wavenumber resolution.

As a result of simulating the unit cell test, the jet flow injected from the jet inlet passed between the columns and showed a turbulent dominant flow that forms eddies of various sizes. It is necessary to reduce a simulation cell size as small as possible for the better prediction of lower plenum flow behavior.

4. CFD results analysis of HTTF lower plenum

4.1. HTTF lower plenum CFD analysis results

The histogram of convective Courant number and wall y + value are shown in Fig. 12(A) and (B). The convective Courant number was calculated to be less than 1 except for very few volumes, and Y+ was calculated to be less than 5. The volume average M value was calculated as0.0916, which is thought to provide more accurate analysis results.

Fig. 13(A)–(C) show the averaged x- and y-velocities and temperature in the section plane at 50% height. As seen in the x-velocity contour, flow separation and vortex shedding were observed behind the column. Since the y-velocity on the far side of the duct is mainly affected by the jet inlet, the velocity in the bottom direction is large, but it decreases closer to the outlet. The temperature profile shows that the average temperature at each side edge is relatively lower than the temperature of center. The low temperature of these edges can lead to a high temperature gradient that causes the hot striking in the direction perpendicular to the jet direction.

The spatial temperature fluctuations are contoured at different heights in Fig. 14(A)–(C). Compared to only the central part, fluctuations were high on the side near the duct at 75% and on the far side at 25% and 50% height. The fluctuation intensity is stronger near the column located near the side rather than at the center, where the thermocouple is mainly attached. However, large fluctuation intensity does not unconditionally cause thermal stress, and frequency domain and amplitude should be analyzed simultaneously through frequency domain analysis, which is dealt with in Section 4.3.

The locations of a total of five data supply lines are shown in Fig. 15. Graphs of the mean x-, y-velocity, and standard deviation for each of the 5 lines are provided in Fig. 16. Through the analysis of the graphs in Fig. 16, it was confirmed that the fluctuation of x- and y-velocity increases as it closer to the outlet duct. For x-velocities, a negative number is a direction that coincides with the mainstream direction. The graph in Fig. 17 provides the average e temperature and pressure across the measurement lines. Through the analysis of the graphs in Fig. 17, it was confirmed that the temperature deviation was larger the farther from the center line and the farther from the outlet duct.

Fig. 18 shows the calculated velocity, temperature, pressure, and their respective variances for all TFs at 25% and 75% height. In the graph of Fig. 18 (A), the velocity of helium was low, but the fluctuation value was high. This means that the entire lower plenum has a turbulence dominant flow characteristic with a large turbulence intensity. Fig. 18 (B) graph shows the average temperature and temperature fluctuation characteristics. Through the graph, regions near TF#5, 6, 11, and 12 can be analyzed as regions with large temperature fluctuations, that is, regions where hot and cool helium gases are not well mixed. Fig. 18 (C) shows the gauge pressure and its standard deviation.

4.2. Vortex identification of HTTF lower plenum

Vortex visualization enables in-depth analysis of the entire flow field. By visualizing the vortex core, the size and type of the vortex center can be analyzed. Compared to 3D streamline or 2D plot, it enables to analyze the flow structure more accurately. Considering the rotational component of the velocity gradient, the vortex can be visualized using Q-criterion. The Q-criterion well defines the vortex core even at low Reynolds numbers, as opposed to the pressure minimum criterion [25]. The definition of Q is:

$$Q = \frac{1}{2}\left(\|\Omega\|^2 - \|\boldsymbol{S}\|^2\right)$$

Where $\|\boldsymbol{\Omega}\| = [\mathrm{tr}(\boldsymbol{\Omega}\boldsymbol{\Omega}^t)]^{1/2}$, $\|\mathbf{S}\| = [\mathrm{tr}(\mathbf{S}\mathbf{S}^t)]^{1/2}$, $\boldsymbol{\Omega}$ and $\mathbf{S}$ stands for the antisymmetric and symmetric components of ∇u, respectively.

The overall vortex structure can be seen in Fig. 19, and a total of 4*2 vortex cores were identified near the outlet duct. Fig. 19(A) shows a perspective view of the vortex core structure near the outlet duct, and it can be seen that one stagnant vortex flows into the outlet duct and forms a longitudinal vortex structure. Second, it

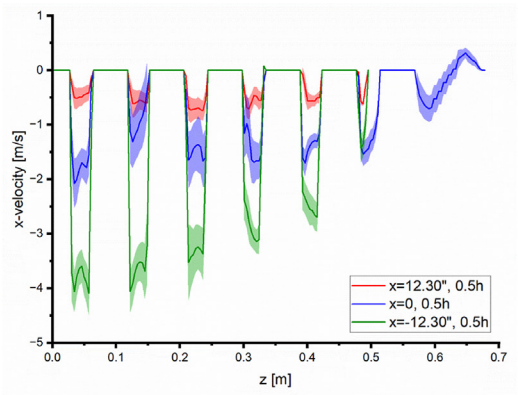

(A) x-velocity at 0.5h, x=12.30", 0, -12.30"

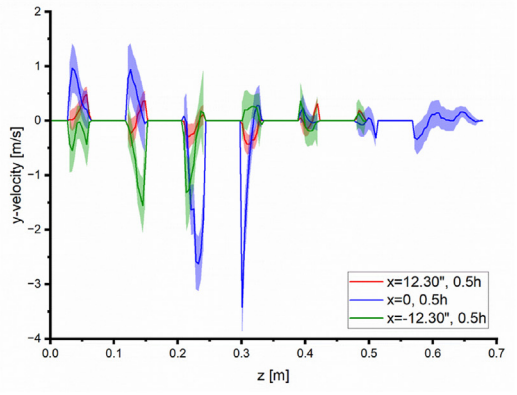

(E) y-velocity at 0.5h, x=12.30", 0, -12.30"

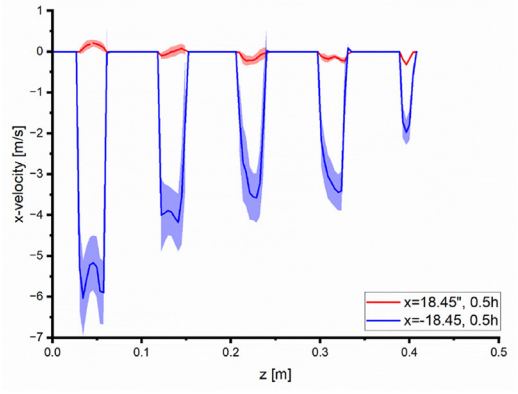

(B) x-velocity at 0.5h, x=18.45", -18.45"

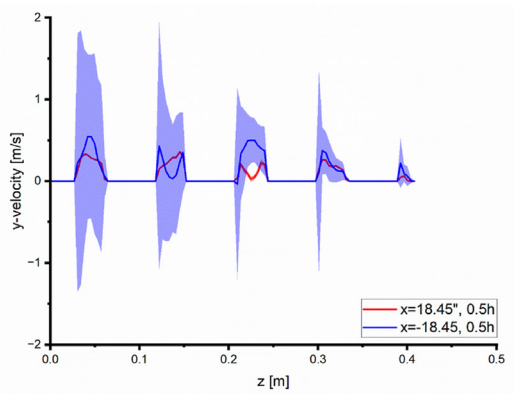

(F) y-velocity at 0.5h, x=18.45", -18.45"

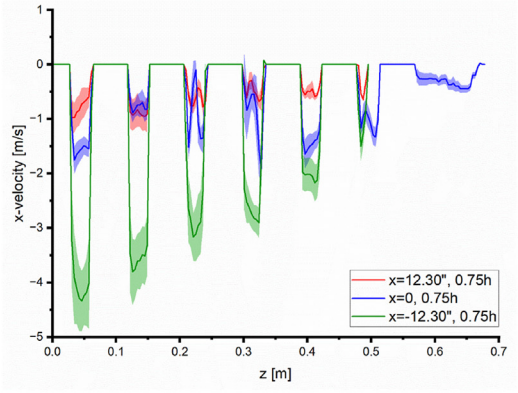

(C) x-velocity at 0.75h, x=12.30", 0, -12.30"

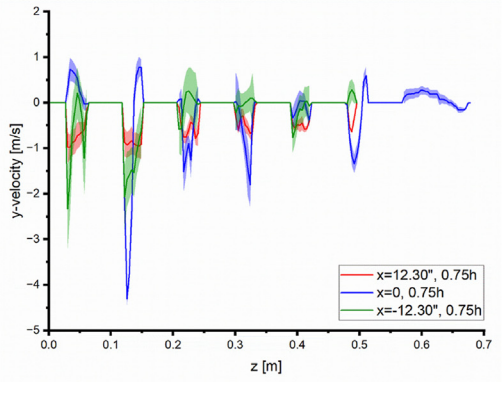

(G) y-velocity at 0.75h, x=12.30", 0, -12.30"

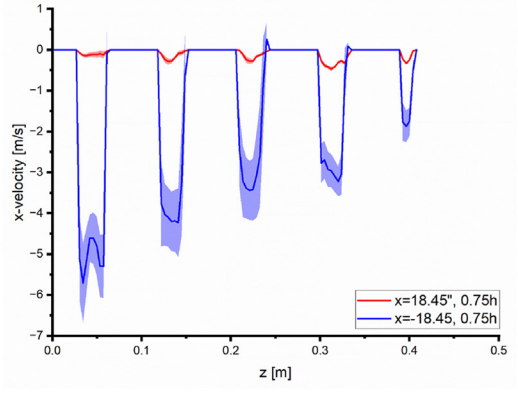

(D) x-velocity at 0.75h, x=18.45", -18.45"

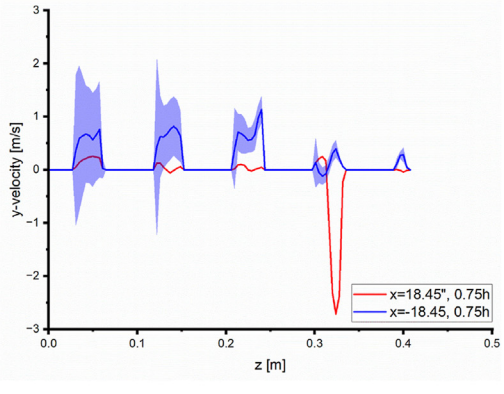

(H) y-velocity at 0.75h, x=18.45", -18.45"

Fig. 16. Mean x-, y-velocity with error range at measurement lines.

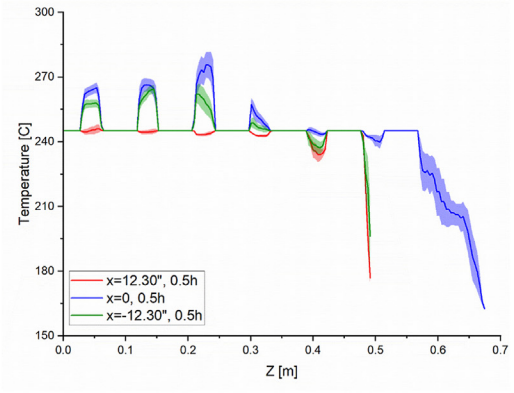

(A) Temperature at 0.5h, x=12.30", 0, -12.30"

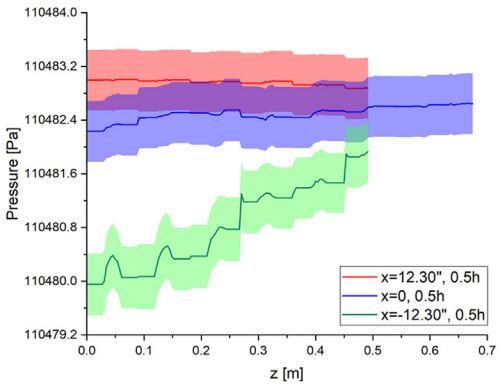

(E) Pressure at 0.5h, x=12.30", 0, -12.30"

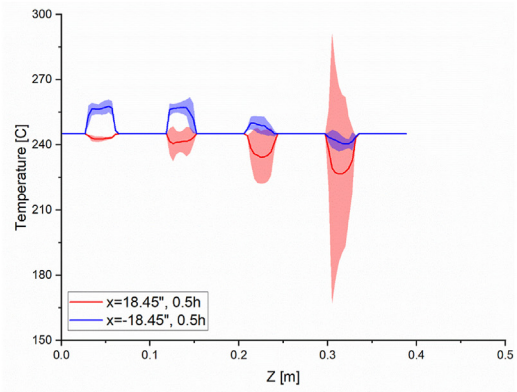

(B) Temperature at 0.5h, x=18.45", -18.45"

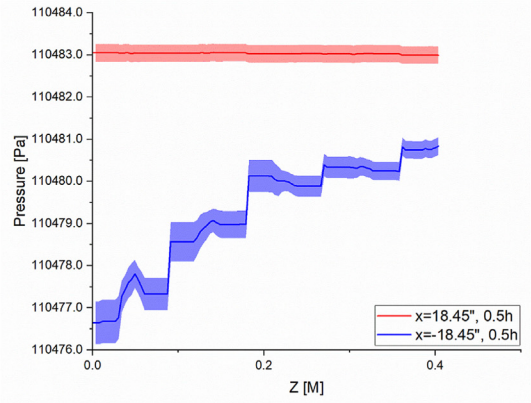

(F) Pressure at 0.5h, x=18.45", -18.45"

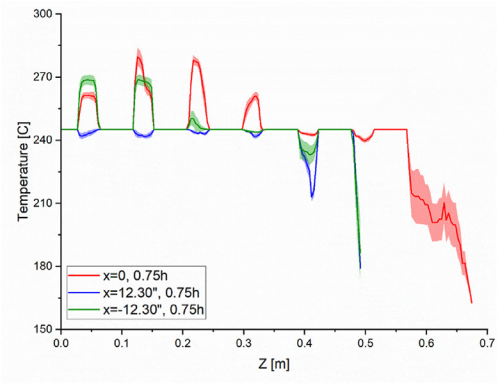

(C) Temperature at 0.75h, x=12.30", 0, -12.30"

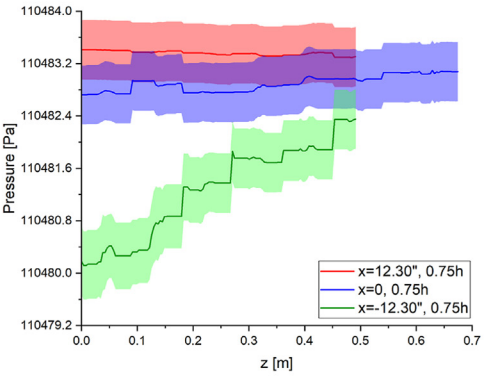

(G) Pressure at 0.75h, x=12.30", 0, -12.30"

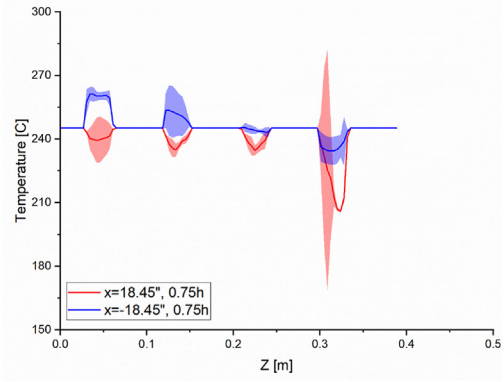

(D) Temperature at 0.75h, x=18.45", -18.45"

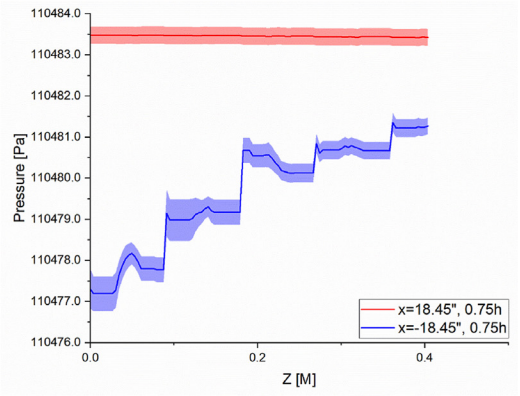

(H) Pressure at 0.75h, x=18.45", -18.45"

Fig. 17. Mean temperature and pressure with error range at measurement lines.

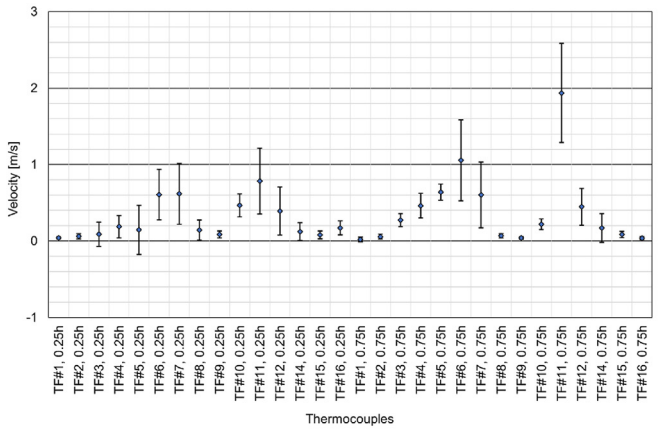

(A) Mean velocity

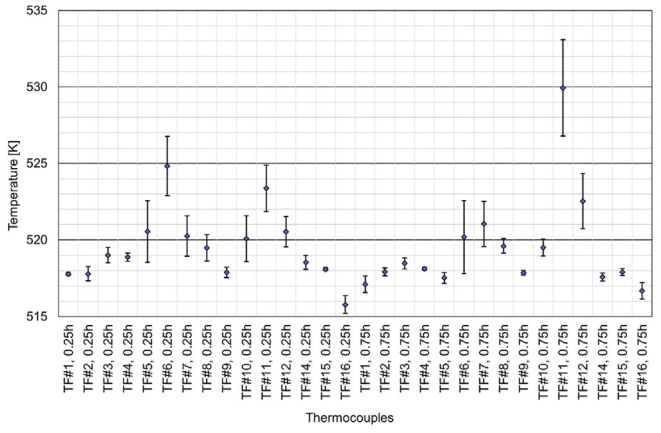

(B) Mean temperature

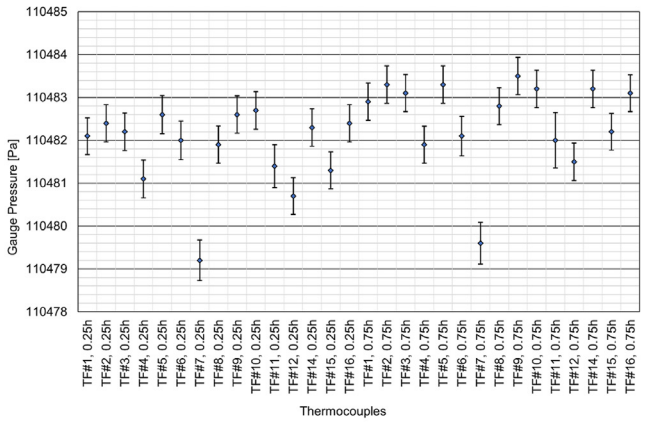

(C) Mean gauge pressure

Fig. 18. Simulated mean variables and variances at thermocouples of lower plenum.

was observed that the longitudinal vortex core was formed from the top of the column near the outlet to the duct. Finally, one stagnant vortex flow generated from the bottom of the outlet and one vortex generated from the side of the duct a little further away were observed. Fig. 19(B) depicts an iso-surface filtered with a Q_{max} of 0.2% in a side view of the lower plenum, revealing three vortexes. The first is the vortex flow formed in the jet inlet, which, as expected, does not affect the depth of the lower plenum as it goes to the wake. The second is a stagnant vortex structure that occurs when helium gas collides with the column wall, and the vortex core can be clearly observed as it goes to the wake. Finally, the horseshoe vortex formed along the bottom surface of the support structure was identified.

5. Fast Fourier Transform analysis of HTTF lower plenum

In order to analyze thermal striping, it is necessary to investigate frequency and amplitude in the frequency domain. Discrete Fourier Transform (DFT) is an algorithm that converts discretized time domain data into discretized frequency domain data. FFT is an algorithm that quickly computes DFT using periodicity and symmetry. FFT can convert a signal into the digital frequency domain. FFT analysis was performed to investigate the risks associated with thermal striping due to jet mixing behavior or hot striking. It should be noted that this study did not couple the analysis of structural parts, so it only investigated the frequency of temperature fluctuations in the fluid part near the wall. Average power P is defined:

$$P = \lim_{T\to\infty}\frac{1}{T}\int_{-\infty}^{\infty}|x_T(t)|^2 dt$$

According to the Parseval's theorem,

$$P = \lim_{T\to\infty}\frac{1}{T}\int_{-\infty}^{\infty}|\hat{x}_T(f)|^2 df$$

Power spectral density (PSD):

$$S_{xx}(f) = \lim_{T\to\infty}\frac{1}{T}|\hat{x}_T(f)|^2$$

Fig. 20(A)–(E) show the FFT analysis result graphs, and the selected TFs are those with high temperature variance values in Fig. 20. There was no specific dominant frequency in the temperature fluctuations of all TFs. TF#5 in Fig. 20(A) is located far from the outlet duct and where the flow rate is not high. At 25% height, the PSD amplitude of TF#5 tends to be higher by a power of 10 compared to 75% height. Fig. 20(B)–(E) show TFs near the outlet duct, and the PSD amplitude at 75% height is greater than at 25% height. In addition, TF#6, 11 installed at a location where the flow is stagnant, was calculated to have a higher PSD amplitude at a low frequency of 10 Hz or less than TF#7, 12 at 75% height. As a result, the highest PSD amplitude was calculated as TF#5 at 25% height and TF#6 and TF#11 at 75% height.

Since it was confirmed that there was a large temperature fluctuation in the corner of the lower plenum, FFT was performed at the points shown in Fig. 15 to analyze the temperature fluctuation characteristics near the column wall. The results of FFT analysis of temperature fluctuations at heights of 25%, 50%, and 75% at 13 points were compared, and P10 and 11 showed the largest PSD amplitude. The FFT results analyzed in P10 and 11 are shown in Fig. 21(A) and (B). It was confirmed that P10 have a relatively high PSD at low-frequency, and P11 was distributed in the frequency region of 10 Hz or higher. As a result, PSD was higher in the two columns located at the corner close to the outlet duct than in the columns located at the other corner, but temperature fluctuation characteristics similar to those of the support structures located in the center were observed.

6. Conclusion

This study provides the results of high fidelity CFD analysis using the LES model to provide quantitative information on the

(A) Outlet duct – Perspective view

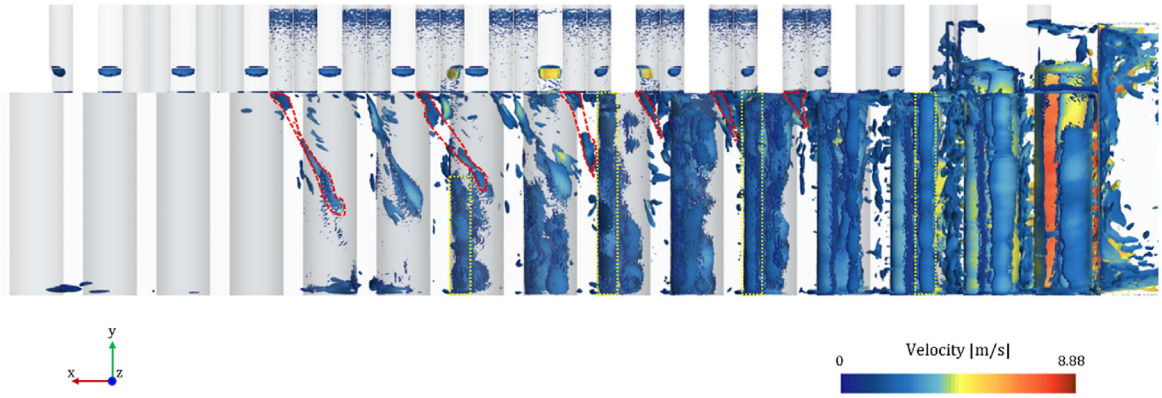

(B) Lower plenum – Side view

Fig. 19. Vortex structure of lower plenum – 0.2% of Qmax.

thermal hydraulic behavior in the HTTF lower plenum. Since helium gas is colorless and odorless, it is difficult to analyze the flow characteristics of the overall flow field through experiments. To compensate for this, the vortex core was visualized for the LES results and the accurate flow field was analyzed. In order to analyze the thermal striping, the temperature fluctuation was analyzed in the frequency domain through the FFT analysis. Key findings from this study are as follows:

1. The LES analysis of the unit cell test of the VTR lower plenum was conducted to establish the baseline CFD model. It was confirmed that the accuracy of CFD prediction was improved as the dependence of the sub-grid scale model decreased.
2. The CFD analysis results for HTTF were quantitatively analyzed. Averaged data for temperature, velocity, and pressure at locations including thermocouples, which can serve as reference data for code-code comparisons, are provided in this study with standard deviations.
3. CFD simulation results using the LES model were qualitatively analyzed, and vortex identification was performed through vortex visualization using Q-criterion. As a result of the vortex identification, the vortex cores that flowed to the duct outlet and the vortex cores that occurred near the support structures of the lower plenum were identified.
4. Frequency domain analysis of temperature fluctuations at thermocouple positions was performed through Fourier fast transform. It was confirmed that thermal mixing in the HTTF lower plenum was not dominant at a specific frequency. The FFT results for thermocouples with relatively high PSD amplitude showed that the overall PSD amplitude of the upper part increased as it went to the wake.
5. The temperature fluctuation was large in the vicinity of the corner of the lower plenum. The FFT analysis for the region in the vicinity of the support structure located at the corner showed that the temperature fluctuation amplitude was not particularly high near the support structure wall.

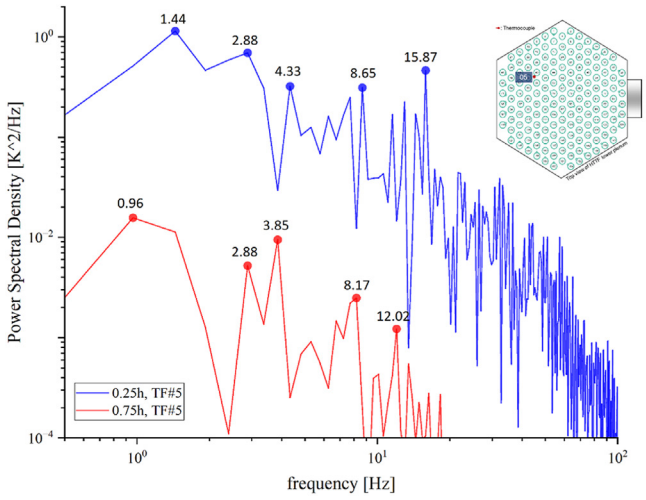

(A) TF#5

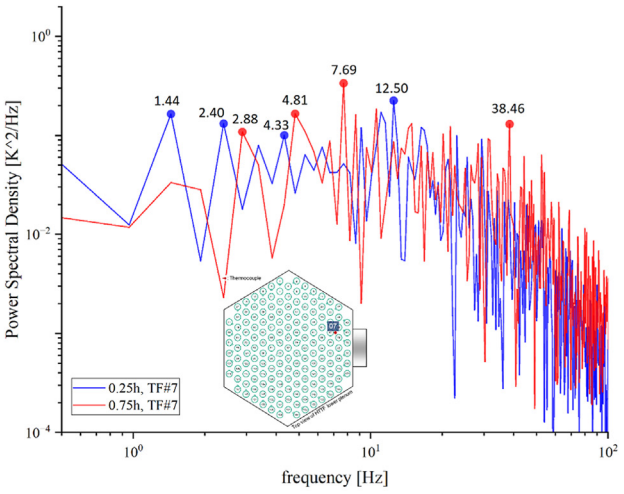

(C) TF#7

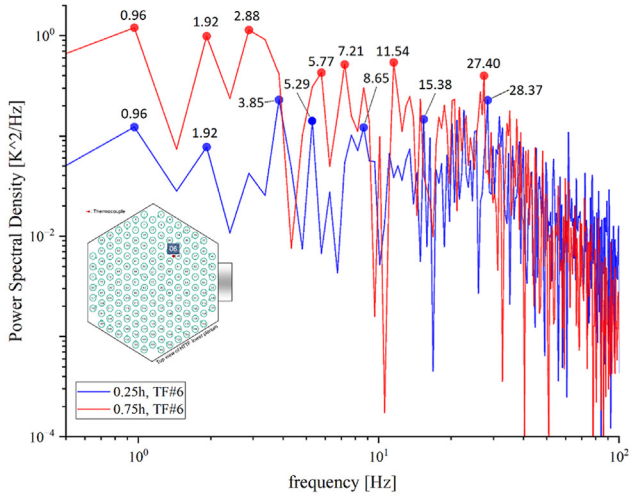

(B) TF#6

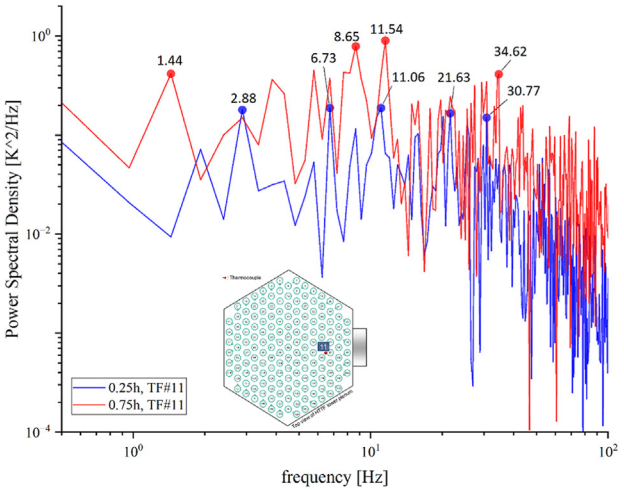

(D) TF#11

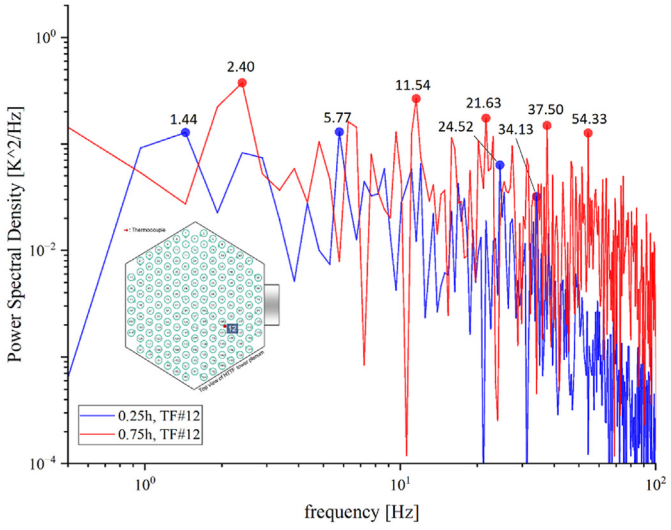

(E) TF#12

Fig. 20. FFT analysis result for temperature of 5 TFs.

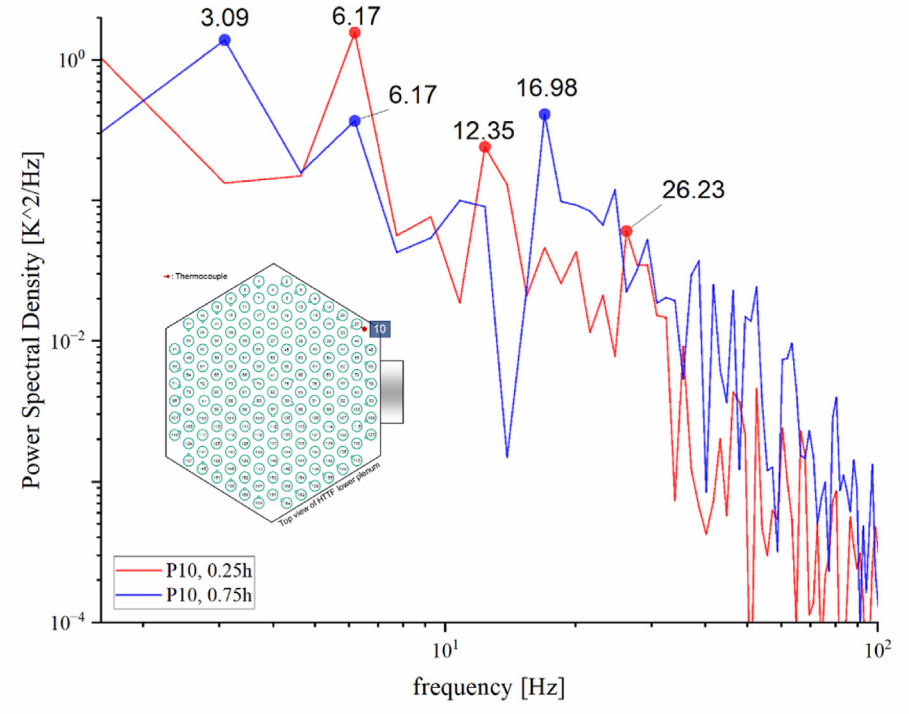

(A) P10

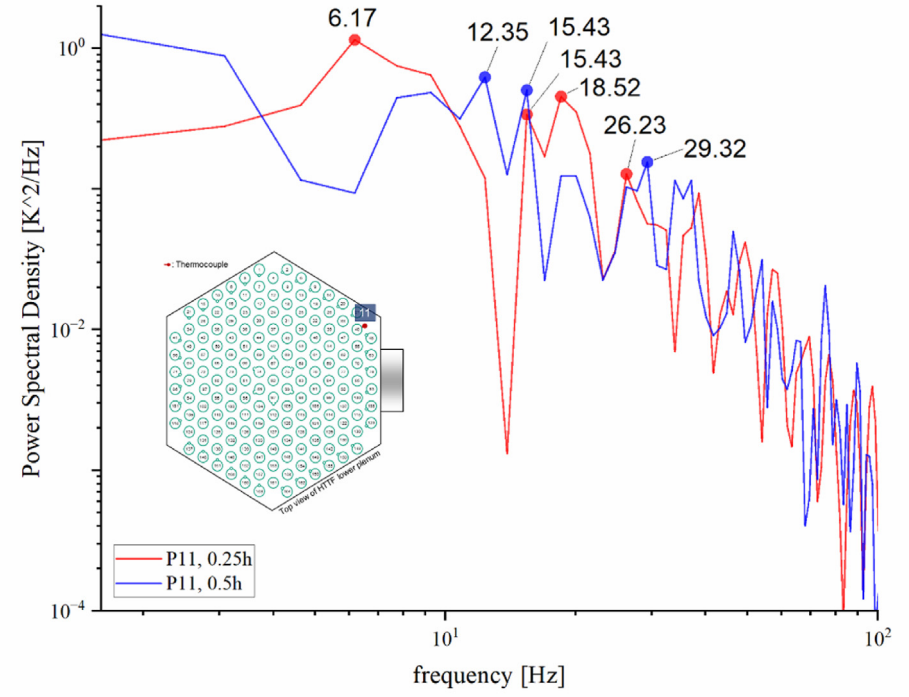

(B) P11

Fig. 21. FFT analysis result for temperature of 2 points.

This study was conducted to provide high-precision flow field data for OECD NEA's HTTF benchmark steady-state calculation and code-code comparison and verification. Institutions participating in the benchmark perform analysis using the RANS base model, and the results of this study can be reference data for verifying the CFD analysis results using the RANS model. In addition, constant helium properties were applied to eliminate interpolation errors that may occur in each code of the benchmark participating institutions.

Declaration of competing interest

The authors declare that they have no known competing financial interests or personal relationships that could have appeared to influence the work reported in this paper.

Acknowledgement

This work was supported by Korea Institute of Energy Technology Evaluation and Planning (KETEP) grant funded by the Korea government (MOTIE) (20214000000780, Methodology Development of High-fidelity Computational Fluid Dynamics for next generation nuclear power), (RS-2023-00243201, Global Talent Development project for Advanced SMR Core Computational Analysis Technology Development). This research made use of the resources of the High Performance Computing Center at Idaho National Laboratory, which is supported by the Office of Nuclear Energy of the U.S. Department of Energy and the Nuclear Science User Facilities under Contract No. DE-AC07-05ID14517.

References

[1] D.M. McEligot, G.E. McCreery, Fundamental Thermal Fluid Physics of High Temperature Flows in Advanced Reactor Systems, Idaho National Laboratory, Idaho Falls, ID, 2002.
[2] S.J. Ball, S.E. Fisher, Next Generation Nuclear Plant Phenomena Identification and Ranking Tables (PIRTs) Volume 1: Main Report", Oak Ridge National Laboratory, Oak Ridge, TN, 2007.
[3] Sal, et al., Numerical investigation of potential elimination of 'hot streaking' and stratification in the VHTR lower plenum using helicoid inserts, Nucl. Eng. Des. 240 (2010) 995–1004.
[4] M.J. Gradecka, B.G. Woods, Development of thermal mixing enhancement method for lower plenum of the High Temperature Test Facility, Nucl. Eng. Des. 305 (2016) 81–103.
[5] D.M. McEligot, G.E. McCreery, Scaling Studies and Conceptual Experiment Designs for NGNP CFD Assessment, Idaho National Laboratory, Idaho Falls, ID, 2004.
[6] K.G. Condie, G.E. McCreery, H.M. McIllroy, D.M. McEligot, Development of an Experiment for Measuring Flow Phenomena Occurring in a Lower Plenum for VHTR CFD Assessment, Idaho National Laboratory, Idaho Falls, ID, 2005.
[7] W.J. Richard, Modeling strategies for unsteady turbulent flows in the lower plenum of the VHTR, Nucl. Eng. Des. 238 (2007) 482–491.
[8] D.P. Guillen, Computational flow predictions for the lower plenum of a high-temperature, gas-cooled reactor, Trans. Am. Nucl. Soc. 95 (2006) 827–828.
[9] B.G. Woods, OSU High Temperature Test Facility Technical Design Report, OSU-HTTF-TECH-003-R1, Rev. 1, Oregon State University, 2017.
[10] Stone & Webster Engineering Corp, Preliminary Safety Information Document for the Standard MHTGR." HTGR-86-024, Department of Energy, 1986.
[11] I. Gutowska, B.G. Woods, S.R. Cadell, CFD modeling of the OSU High Temperature Test Facility inlet plenum flow distribution during normal operation, NED 353 (2019), 110216.
[12] K. Podila, Q. Chen, Coupled simulations for prismatic gas-cooled reactor, NED 395 (2022), 111858.
[13] Siemens Digital Industries Software, Simcenter Star-CCM+ User Guide, Siemens, 2022, version 2022.1.
[14] Y.Q. Yu, E. Merzari, Steady and unsteady calculations on thermal striping phenomena in triple-parallel jet, NED 312 (2017) 429–437.
[15] S. Chacko, Y.M. Chung, Large-eddy simulation of thermal striping in unsteady non-isothermal triple jet, Int. J. Heat Mass Tran. 54 (2011) 4400–4409, 2011.
[16] D. Tyler Landfried, Kristo Paul, Design of an experimental facility with a unit cell test section for studies of the lower plenum in prismatic high temperature gas reactors, Ann. Nucl. Energy 133 (2019) (2019) 236–24.
[17] Corey E. Clifford, Austen D. Fradeneck, Computational study of full-scale VHTR lower plenum for turbulent mixing assessment, 2019, Annals of Nuclear Energy 134 (2019) 101–113.
[18] Sasan Salkhordeh, Corey Clifford, Large Eddy Simulations of scaled HTGR lower plenum for assessment of turbulent mixing, NED 334 (2018) 24–41.
[19] Mark Kimber, John Brigham, Anirban Jana, Experimentally Validated Numerical Models of Non-isothermal Turbulent Mixing in High Temperature Reactors, United States: N. p., 2018 https://doi.org/10.2172/1461189. Web
[20] J.E. Brdina, P.G. Huang, T.J. Coakley, Turbulence modeling validation, testing and development, NASA Tech. Memo. 110446 (1997) 147.
[21] D.C. Wilcos, Re-assessment of the scale-determining equation for advanced turbulence models, AIAA J. 26 (1988) 1299–1310.
[22] F.R. Menter, Two-equation eddy-viscosity turbulence models for engineering applications, AIAA J. 32 (1994) 1598–1605.
[23] F. Ducros Nicoud, Subgrid-scale stress modelling based on the square of the velocity gradient tensor, Flow, Turbul. Combust. 62 (1999) 183–200.
[24] J. Smagorinsky, General circulation experiments with the primitive equations I. The basic experiment, Mon. Weather Rev. 91 (1963) 99–164.
[25] F. Hussain, On the identification of a vortex, JFM 285 (1995) 69–94.